Analog RF Circuit for an Open-Hardware Vector Network Analyser

EE3L11: Bachelor Graduation Project

R.Dirkzwager and S. Öztürk

Analog RF Circuit for an Open-Hardware Vector Network Analyser

by

R.Dirkzwager and S. Öztürk

in partial fulfilment of the requirements for the degree of

Bachelor of Science

in Electrical Engineering

to be defended Friday 21 June, 2024 at 11:30.

Students:	Ruben Dirkzwager	5608821
	Samet Öztürk	5324440
Project Supervisor:	Prof.dr. G. Steele	TU Delft
EEMCS Supervisor:	Dr.ir. N. Haider	TU Delft
Thesis committee:	Dr.ing. I. E. Lager	TU Delft
	Prof.dr. G. Steele	TU Delft
	Dr.ir. N. Haider	TU Delft
	Dr. S.M. Alavi	TU Delft

Style: TU Delft Report Style, with modifications by D. Zwaneveld and M.J.A. Langenberg

TU Delft

Preface

The last two months have been dedicated to working on the bachelor thesis you have in front of you. This project, conceived by Gary Steele, has involved tremendous effort to present a working prototype and to prove the concept.

We would like to extend our heartfelt thanks to Gary Steele and Nadia Haider for their invaluable support and guidance, which were instrumental in making this project a success in our eyes. We are proud of how far we have come and how much we have learned over this period.

Additionally, we want to thank Simon Schaap, Maarten Oudijk, Anne Hinrichs, and Matthijs Langenberg for their excellent teamwork and collaboration throughout this project.

R.Dirkzwager and S. Öztürk
Delft, June 2024

Abstract

This thesis presents the design, implementation, and evaluation of the RF (Radio Frequency) section of an Open-Hardware Vector Network Analyzer (VNA) intended for quantum research applications. The project aims to create a cost-effective, modular VNA system that fulfills the functional requirements necessary for qubit readout and other quantum measurements.

In the initial chapters, the overall architecture of the VNA is outlined, with specific attention to the power budget and system requirements. The RF generation principles are examined, and a range of RF generators are tested to ensure they meet the signal quality standards, such as spurious emissions and harmonic content. The performance of various RF mixers is also evaluated and found to be sufficient for the RF system.

Experimental results demonstrate the system's capability to measure the S_{21} parameter of a resonator cavity, comparable to commercial VNAs. This validates that the RF system meets the specified requirements and can be effectively used in quantum research.

Future work suggested includes the measurement of generator frequency/phase stability over time and exploring the feasibility of implementing power sweeps to enhance the system's functionality. The findings of this thesis contribute to the development of accessible and flexible tools for quantum technology research, promoting further advancements in the field.

Contents

Nomenclature

Abbreviations

Abbreviation	Definition
ACI	Adjacent Channel Interference
ADC	Analog to Digital Converter
API	Application Programming Interface
DAC	Digital to Analog Converter
DC	Direct Current
DR	Dynamic Range
DSP	Digital Signal Processor
DUT	Device Under Test
EM	ElectroMagnetic
EMW	ElectroMagnetic Wave
FPGA	Field Programmable Gate Array
GUI	Graphical User Interface
IF	Intermediate Frequency
IFBW	Intermediate Frequency Bandwidth
IQ	In-phase and Quadrature
LO	Local Oscillator
LSB	Least Significant Bit
PCB	Printend Circuit Board
PD	Phase Detector
PLL	Phase Locked Loop
PTFE	PolyTetraFluoroEthylene
REF	Reference
RF	Radio Frequency
RL	Return Loss
SDR	Software Defined Radio
SFDR	Spurious Free Dynamic Range
SMA	SubMiniature version A
SNR	Signal to Noise Ratio
SoC	System on Chip
TDR	Time Domain Reflectometry
VCO	Voltage Controlled Oscillator
VNA	Vector Network Analyser
WFT	WindFreakTech

1

Introduction

1.1. VNA, a general overview

A VNA is a device that sends an electromagnetic wave (EMW) at a known frequency and amplitude through a DuT or network, and records the reflected and transmitted waves[1]. The recorded waves are compared to the transmitted wave to derive a vector output, giving the change in amplitude and phase caused by the DuT.

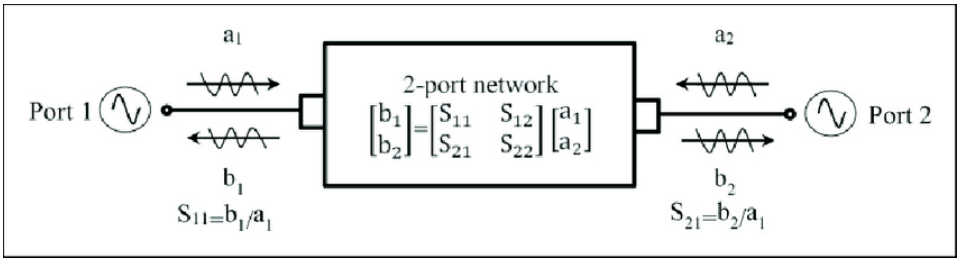

Figure 1.1: S-parameters [2]

The reflected EMW, transmitted EMW and the EMW that is sent by the VNA, which from now on can be referred to as the reference signal, can be represented using two sinusoidal waves: an in-phase cosine (I), and a sine, shifted by 90 degrees compared to I, referred to as the quadrature wave (Q). These waves are combined to form a complex mathematical IQ representation: $I + \mathrm{j}Q$.

The change caused by a DuT in its reflection and transmission of the reference signal are quantified by scattering parameters, or S-parameters, which are a form of network parameters. For a two-port DuT, the S-parameters can be shown as a 2×2-matrix [3], shown in figure 1.1. These parameters contain information about both the phase and amplitude change caused by the DuT, in a complex form. They are obtained by complex division of the reflected or transmitted signal by the reference signal, such as in equation (1.1).

$$S_{21} = \frac{b_2}{a_1} = \frac{I_{\text{trans}} + \mathrm{j}Q_{\text{trans}}}{I_{\text{ref}} + \mathrm{j}Q_{\text{ref}}} \tag{1.1}$$

For this project, this S_{21} transmission parameter is of interest, which relates the transmitted signal (b_2 in figure 1.1) to the reference signal (a_1).

VNAs have two main procedures to test a DuT. The first procedure is called frequency sweep, where an EMW is sent with a constant power and a frequency changing over a short time span. This procedure is used to determine the frequency-dependence of the reflection- and transmission parameters of the DuT. The second procedure is a power sweep, where an EMW is sent with constant frequency and a power changing over a short time span. This procedure is used to determine the power transfer of the DuT at

different input powers. For this project, only the frequency sweep is of interest, and implementation of power sweeping is left to future projects.

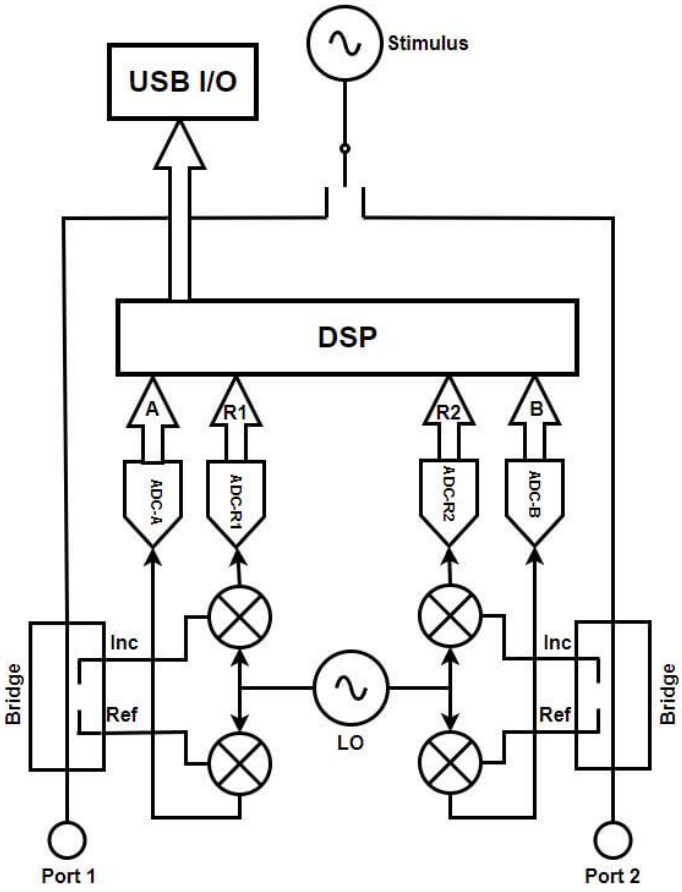

Figure 1.2: Block diagram of a simple VNA, [4]

The internal working of a general simple VNA is shown in figure 1.2. An RF stimulus coming from port 1 is provided to a DuT, which is connected between port 1 and port 2 (not shown in figure 1.2). The stimulus is passed through a bridge (directional coupler), which splits the EMW in forward- and backward-going waves, which takes this signal as reference (Ref). This reference signal is made into a lower frequency IF-signal (intermediate frequency) by a mixer using a local oscillator (LO). The intermediate frequency is determined by the difference in frequency of the LO and the incoming signal. The reflected EM wave coming from the DuT will be split off as the ”Inc”-signal by the bridge at port 1, and the transmitted wave as the ”Inc”-signal at port 2. They then go through the same process as the reference signal, to obtain 2 more IF-signals. The same process can also be done with a RF-stimulus coming from port 2, producing another reference, transmission and reflection IF-signal, to study the directional effects of the DuT.

All IF-signals are then digitised in Analog-to-Digital Converters (ADCs) and processed in the Digital Signal Processing unit (DSP). In the DSP, the 4 S-parameters are calculated by doing the complex divisions such as the one in equation 1.1. After that, the data can be retrieved via a data bus such as USB, or be immediately shown on a screen.

1.2. Application in quantum research

A Transmon qubit is a type of superconducting charge qubit. It consists of a superconducting quantum interference device (SQUID), a non-linear inductive element made of two superconductors separated

by a thin insulating barrier, and a shunting capacitor C_t. The SQUID consists of two Josephson junctions in a loop. The Josephson junctions provide the non-linear inductance necessary to create quantised energy levels with nonuniform spacing (also known as anharmonicity). Anharmonicity is the key to confining the dynamics of multi-level quantum system (such as a Transmon) to within a two-level subspace when it is driven.

Being able to confine the dynamics within a two-level subspace is important because it simplifies the system to a manageable quantum bit, or qubit, which is the fundamental unit of information in quantum computing. This confinement allows for clear distinction between the two states, 0 and 1, necessary for reliable quantum operations and algorithms. It also reduces the likelihood of leakage into higher energy states, which can lead to errors and decoherence, thus improving the overall stability and performance of quantum circuits. The primary role of the shunting capacitor is to increase the charging energy relative to the Josephson energy, which mitigates the effects of charge noise and enhances the robustness of the qubit.

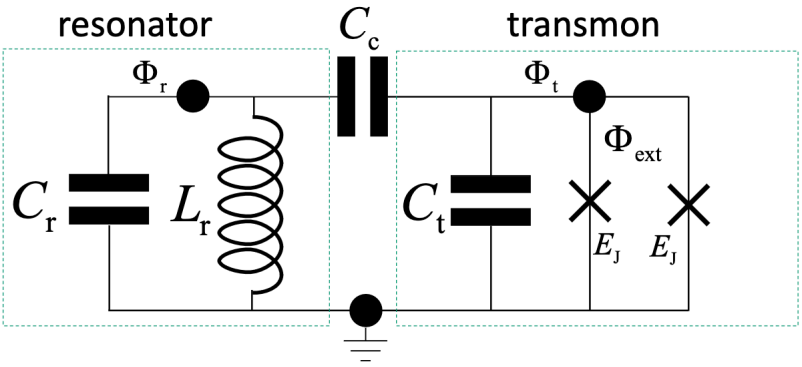

Figure 1.3: Transmon qubit coupled to a resonator [5]

Figure 1.3 shows the lumped element model of the Transmon qubit coupled to a resonator. The resonator is implemented as a waveguide (here modelled as a single inductance and capacitance). The resonator is the mechanism by which the qubit is read out, so it is also called the readout resonator.

The key to the microwave readout is sending a calibrated microwave pulse towards the resonator. This pulse is typically set at or near the resonator's base frequency ω_r , but the qubit-state-dependent frequency shift (either $\omega_r - \chi$ or $\omega_r + \chi$) affects how this pulse interacts with the resonator. The way this is done in practice is by the use of a VNA. Qubit measurement can be performed by taking the superconducting qubit circuit as the DuT and measuring its S_{21}-parameter. This parameter helps to determine changes in the microwave signal due to the qubit-state-dependent frequency shift, thereby enabling the measurement of the qubit state.

In figure 1.4 an actual picture of the Transmon qubit can be seen, together with the readout resonator and what a successful readout looks like. In figure 1.5 a more schematic representation of the readout procedure is shown.

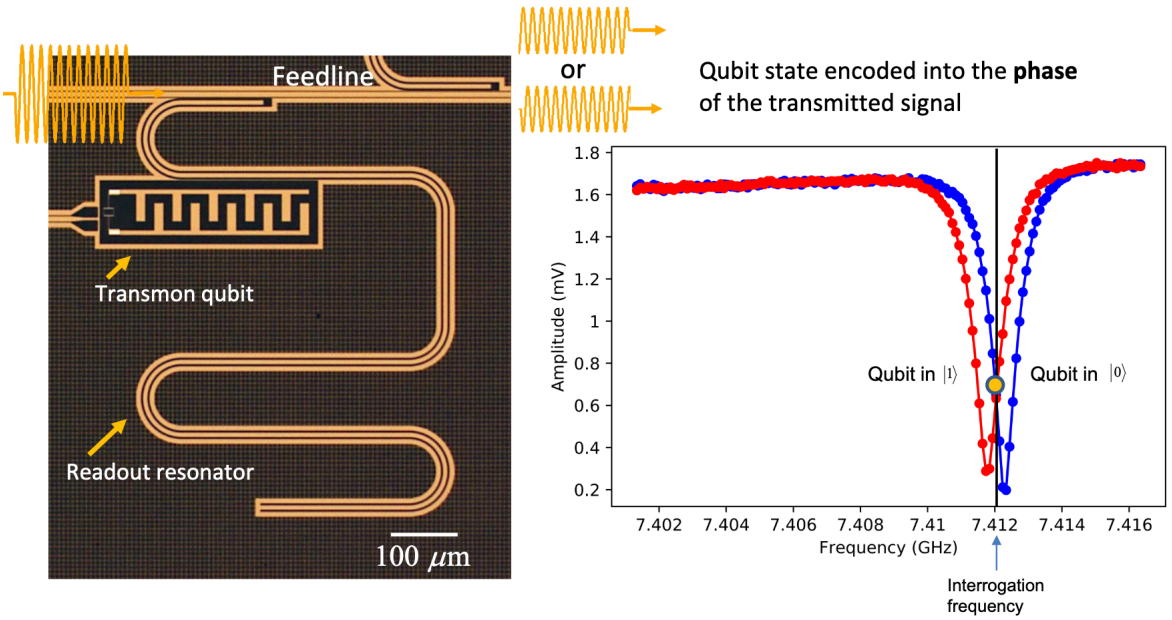

Figure 1.4: Left: Image of a real Transmon qubit and the attached readout resonator. Right: amplitude of transmitted signal through the qubit as a function of applied frequency.[5]

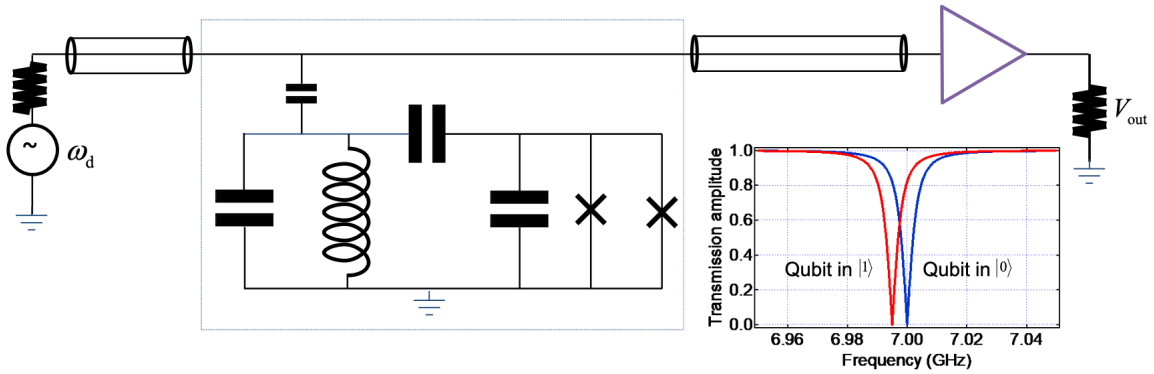

Figure 1.5: Readout of a Transmon qubit [5]

1.3. Existing solutions

Commercial VNAs from companies like Keysight and Tektronix are often quite expensive, having price tags of several tens of thousands of euros [6]. This is in large part due to their accuracy combined with a large frequency range which extends into multiple GHz range, which requires expensive components. Extensibility is provided with equally expensive options, but offer limited flexibility because users are limited to the offerings of the company for that specific model.

Cheaper options are available too, in the price range of a hundred to several hundreds of euros, but these options provide a narrower frequency range and lower accuracy [7]. Being sold in a single package, these options also do not offer much extensibility without having to study the (often open-source) documentation thoroughly.

VNAs are in the field of quantum computing sold as quantum controllers[8][9]. These systems offer most of the flexibility that are required for qubit research, but have prices in the range of hundred thou-

sands of euros. This is the case because of their very high accuracy and very large frequency range.

To offer much higher flexibility than normal VNAs, and low to moderate prices, there have been projects on VNAs using SDR (software defined radio) technology, which recreates (expensive) analog EMW-components in software [10]. This can be done using for example a FPGA (Field Programmable Gate Array) to obtain even higher flexibility and processing speed. An attempt was been made by an hobbyist to create a VNA using SDR-technology on an FPGA [11]. Another attempt was been made that shows an FPGA-based alternative for a VNA used for imaging in industry in the 200 GHz range [12].

Recently, there has also been an effort to create a VNA or quantum controller using SDR-technology on an FPGA [13].

1.4. Functional requirements

The requirements for the VNA of this project select the basic VNA functionality which is most useful for the application of interfacing with qubits. Omitting other functions of a commercial VNA is what makes it possible to offer a cheaper and more modular system. The system can be made using off-the-shelf RF components, an FPGA and a RF signal generator. The layout for the FGPA and the interfacing programs are made open-source, to make the product available for free in the research sector. To make the interaction with the VNA understandable for the researchers, Python code is used for the user interface and API (Application Programming Interface). The quantitative requirements of the entire VNA are shown below:

1. Ability to measure the S_{21}(transmission) parameter.
2. Operating frequency of 4-8GHz
3. Integration time per measurement point:
    - upper limit: up to 1 second (1 Hz IF bandwidth).
    - lower limit: down to 1 ms per point (1 kHz IF bandwidth).
4. Less than 10 % of the sweeping time should be without output.
5. Spurs of the signal going to the device under test are less than 40dbc.

There are also a few qualitative requirements:

1. The system should be responsive for a human user by having a time under 100 ms between a user input/output and a physical event happening.
2. absolute calibration of the device is not important. It will only be used for relative measurements
3. Modularity, the system should work with any generator

1.4.1. Requirements RF system

The specific RF system requirements are mostly derived from the full system requirements and are as follows.

1. Maximum output peak-to-peak voltage of 2V or 10dBm (on a 50 ohm input).
2. Generate a signal that can sweep between 4 to 8 GHz.
3. Downconvert the signal from GHz range to an IF (Intermediant Frequency) of 7.8125 MHz.
4. Spurs of the signal going to the device under test are less than 40dBc.
5. Highest harmonic less than 30dBc
6. Use off the shelve RF components for example: mixers, splitters and generators.

These requirements will be the main framework guiding the development of the subproject.

1.5. Materials

A Red Pitaya STEMlab 125-14 board was used for the FPGA section, which is described as a signal acquisition and generation platform. This device contains a Xilinx Zynq 7010 system on chip (SoC) and several connectors, such as an ethernet port, micro-usb, GPIO-pins and RF SMA connectors. The SoC contains both programmable logic (PL), which is an FPGA, and a processing system (PS), which contains an ARM®-processor.

For the RF section a variety of components by Minicircuits are used and also the following RF generators are used:

- A SynthHD (V2) 10MHz – 15GHz Dual Channel Microwave Generator by Windfreak Technologies, LLC. With its 2 output channels it produced both the RF stimulus signal and the RF LO signal, in one package with a single API. This generator degraded to an extent which made in unusable for the VNA, which is why it was replaced halfway the project by the following 2 RF generators:
- An HMC-T2100 10 MHz - 20 GHz synthesized signal generator by Hittite Microwave Corporation (now from Analog Devices, Inc.), which was used for the stimulus signal.
- An APUASYN20 8 kHz - 20 GHz Ultra-Agile Signal Source by AnaPico AG, which was used as LO.

1.6. Problem definition

To achieve the functional requirements, several engineering problems had to be solved. For this, three teams or subgroups of 2 persons have been formed: the RF-team, the FPGA-team and the software-team. The RF team had to downconvert the RF signals going to the DuT and REF to IF, which the ADC of the FPGA team could digitize. Generators, mixers and power splitters had to be chosen which would work best to achieve the requirements. Moreover the behaviour of these components had to be measured and documented as well as the entire power budget throughout the system.
The signals that were digitized at the input of the Red Pitaya had to be turned into IQ signals by the FPGA team. Averaging was done on the FPGA to achieve the IF bandwidth requirements. Another engineering problem for the FPGA team together with the software team was the communication between the PL and the PS. Data from the FPGA had to be sent to the software team while control instruction from the software team had to be handled. The software team also had to create an interface between the user and the VNA. An API and optionally a GUI (graphic user interface) were developed for this interaction, which ran on a client program written in Python. This client also had to communicate with the PS of the Red Pitaya. A schematic of this arrangement is shown in figure 1.6.

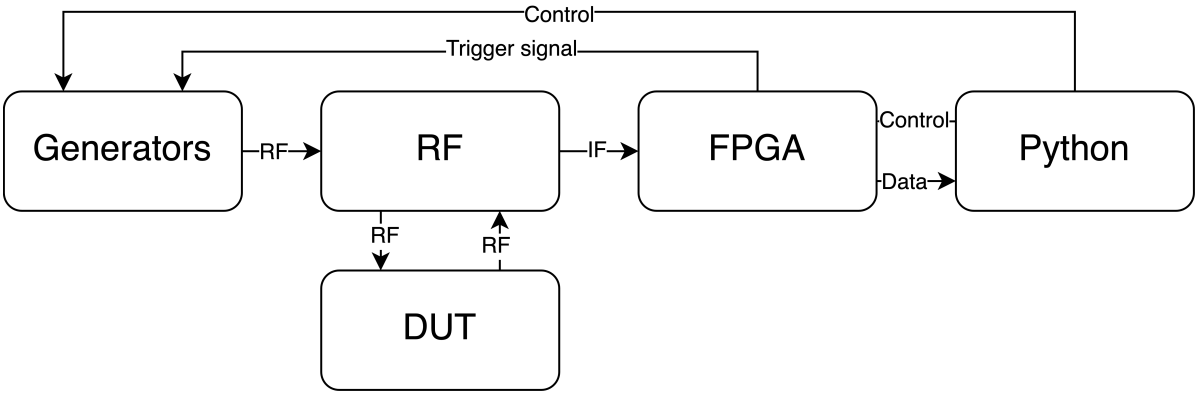

Figure 1.6: Simplified structure of input/output scheme of each subgroup.

1.7. Thesis overview

This thesis is organised into several chapters, each of which plays a crucial role in the overarching structure of the RF part of the VNA. In Chapter 2, we will present an overview of the architectural frameworks. This serves as the foundational basis for the subsequent discussions in the thesis. The chapters that follow delve into various components of the architecture in detail.

Each component section starts with a theoretical discussion that explains the operational principles of the device. This is followed by an examination of the physical implementations, where different approaches to constructing and realising the device are explored. Furthermore, we describe and document various experiments and measurements that have been conducted, providing empirical evidence to support theoretical claims and practical implementations. This methodical approach ensures a comprehensive understanding of each component within the system's architecture. These experiments will also help in supporting the choice in components.

2

Architecture and working principle

In this chapter, the architecture of the RF section of the VNA and its working principle will be detailed, with a focus on the crucial process of RF downconversion, which shifts high-frequency signals to lower frequencies for easier processing. The theoretical foundation and practical implications of high and low side downconversion schemes, the importance of maximizing ADC input power, and the theoretical dynamic range of the ADC will be explained. Additionally, the power budget for the static power architecture will be analyzed, discussing component choices and their impact on overall system performance. Understanding these elements is essential for optimizing the VNA's accuracy and efficiency in signal measurement and analysis.

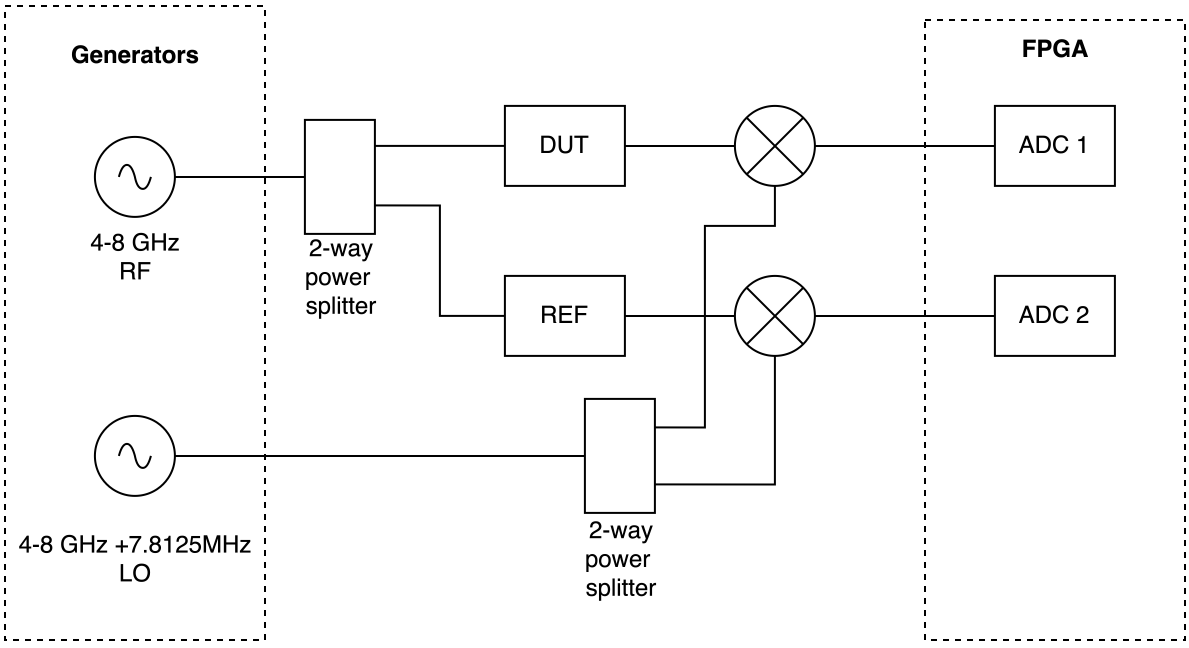

Figure 2.1: Architecture of the RF section of the VNA

2.1. Theory of operation

The theory of operation of the RF section of the VNA primarily follows the principle of RF downconversion. RF downconversion is a process used in communication systems to shift a high-frequency signal (RF) to a lower frequency (IF) to facilitate easier processing. The the mixer can be seen as a circuit element which implements the mathematical function of multiplication. Let's analyse what happens when two cosine functions are mathematically multiplied.

$$S_{RF} = cos(2\pi f_{RF} t)$$
$$S_{LO} = cos(2\pi f_{LO} t)$$
$$S_{RF} \cdot S_{LO} = cos(2\pi f_{RF} t) cos(2\pi f_{LO} t)$$
$$S_{RF+IF} = \cos(2\pi f_{RF} t)$$

$$S_{LO} = \cos(2\pi f_{LO} t)$$

$$S_{RF} \cdot S_{LO} = \cos(2\pi f_{RF} t)\cos(2\pi f_{LO} t)$$

Using the trigonometric identity:

$$\cos(A)\cos(B) = \frac{1}{2}[\cos(A-B) + \cos(A+B)]$$

The following expression is obtained:

$$\cos(2\pi f_{RF} t)\cos(2\pi f_{LO} t) = \frac{1}{2}[\cos(2\pi f_{RF} t - 2\pi f_{LO} t) + \cos(2\pi f_{RF} t + 2\pi f_{LO} t)]$$

Simplifying:

$$\cos(2\pi f_{RF} t)\cos(2\pi f_{LO} t) = \frac{1}{2}\cos(2\pi(f_{RF} - f_{LO})t) + \frac{1}{2}\cos(2\pi(f_{RF} + f_{LO})t)$$

From the derivation it becomes clear that the multiplication of two cosines result in two new signals. One signal (the lower side band) is the difference in arguments (frequency and phase offset) and one signal (the upper side band) is the sum of the arguments. In this application, the lower sideband will be used because it allows for the sampling of the signal, given that the sample rate of the RED Pitaya is not high enough to sample the original RF signal. In figure 2.2 the principle is shown graphically.

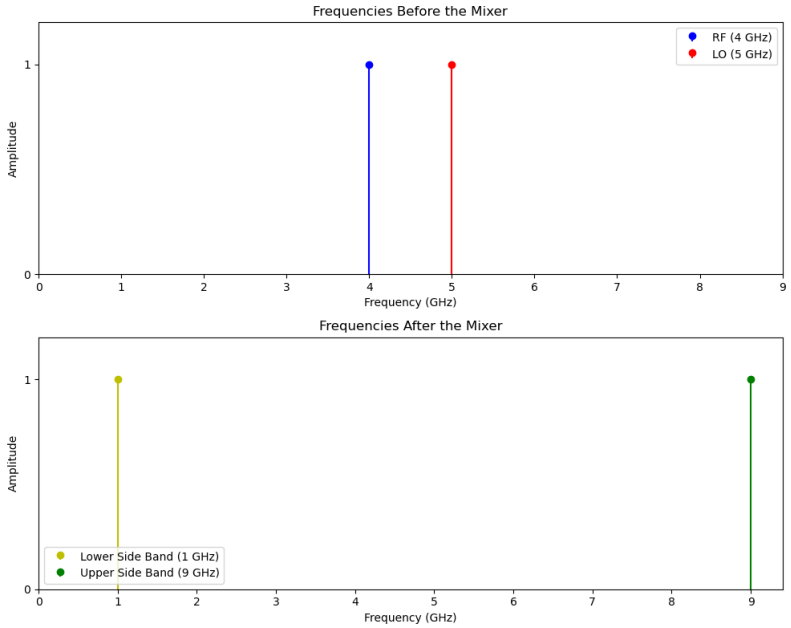

Figure 2.2: Theoretical illustration of downconversion, the difference between RF and LO is called the intermediate frequency. The lower side band (at 1GHz) is the downconverted signal and the upper side band is the upconverted signal (9GHz). Note that the frequencies in the figure are not representative of the actual values used in the architecture.

2.1.1. High or low side downconversion

There are two scheme's possible for choice of LO frequency. One where the LO frequency is lower (low side injection) than RF and one where LO is higher(high side injection). Both result in the same IF frequency after downconversion. The difference is that high side downconversion reflects the lower side band and low side injections does not reflect the lower side band. In the design, the IF is only a single frequency and thus it is not necessary to treat a reflected lower side band. The decision for high or low side injection does not affect the architecture.

2.2. Maximum power at ADC input and dynamic range

2.2.1. Maximum ADC input power

Optimally, it is desired for the peak input voltage signal to match the ADC input range. The ADC that is used is that of the RED Pitaya. It has two possible ADC input range (high and low) with low being 1V peak to peak and high 25V peak to peak. The low input range is used. From the diagram provided

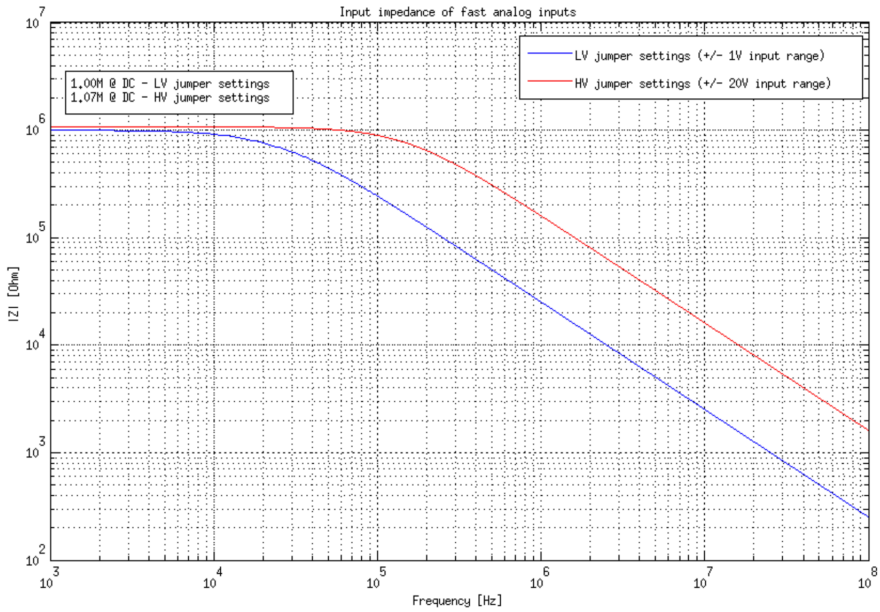

Figure 2.3: RED Pitaya input resistance [14]

by RED Pitaya the magnitude of the input impedance at the IF can be determined. It comes out to be around 2kΩ. To deal with the mismatched impedance, the input is 50Ω terminated with a tee connection. 2kΩ can be approximated as sufficiently larger than the 50 Ω such that it can assumed the input of the ADC to be 50Ω when the input is 50Ω terminated.
To calculate the maximum input power of the ADC the following relation between signal power (in dBm) and voltage over a resistance is used. Where V_{rms} is $\frac{V_p}{\sqrt{2}} = 0.707$V and $|Z_{in}|$ is now the aforementioned 50Ω.

$$P_{inmax} = 10log(\frac{V_{rms}^2}{|Z_{in}| * 0.001}) \tag{2.1}$$

This results in a maximum input power of the ADC of **+10dBm**.

2.2.2. Theoretical dynamic range

To calculate the theoretical maximum dynamic range (DR) of an analog-to-digital converter (ADC), one starts by understanding the range of voltage levels it can measure. For an ADC, the dynamic range is the ratio of the maximum input signal to the minimum detectable signal, which corresponds to the

voltage value of the least significant bit (LSB). The ADC used in the project is the built in ADC of the Red Pitaya which has a resolution of 14 bits.

An N-bit ADC divides the full-scale voltage range (V_{FS}) into 2^N discrete levels. Each quantization level corresponds to a specific voltage step..

For an ADC with a full-scale range of V_{FS} volts, the LSB is:

$$\Delta = \frac{V_{\text{FS}}}{2^N}$$

The dynamic range is the ratio of the maximum input signal to the minimum detectable signal (which is the voltage value of the LSB). This ratio can be expressed as:

$$\text{DR} = \frac{V_{\text{max}}}{\Delta}$$

Since $V_{\text{max}} = V_{\text{FS}}$:

$$\text{DR} = \frac{V_{\text{FS}}}{\frac{V_{\text{FS}}}{2^N}} = 2^N$$

To express the dynamic range in decibels (dB), a logarithmic conversion is used:

$$\text{DR} = 20 \log_{10}(2^N)\ [dB]$$

For a 14-bit ADC, substituting $N = 14$ into the derived formula the dynamic range of the ADC is:

$$\text{DR} = 84.28\ [dB]$$

Therefore, the theoretical maximum dynamic range of a 14-bit ADC is 84.28dB. This result indicates the range over which the ADC can effectively differentiate the smallest and largest input signals based on the voltage value of the LSB and the maximum input signal.

2.3. Power budget static power architecture

The most straightforward implementation of the power budget is the static power approach, which does not incorporate variable gain stages. This section provides an overview of the losses within the architecture. The analysis focuses on the component losses of the final components, with detailed component choices discussed in later chapters. For an in-depth analysis of component selection, please refer to those chapters.

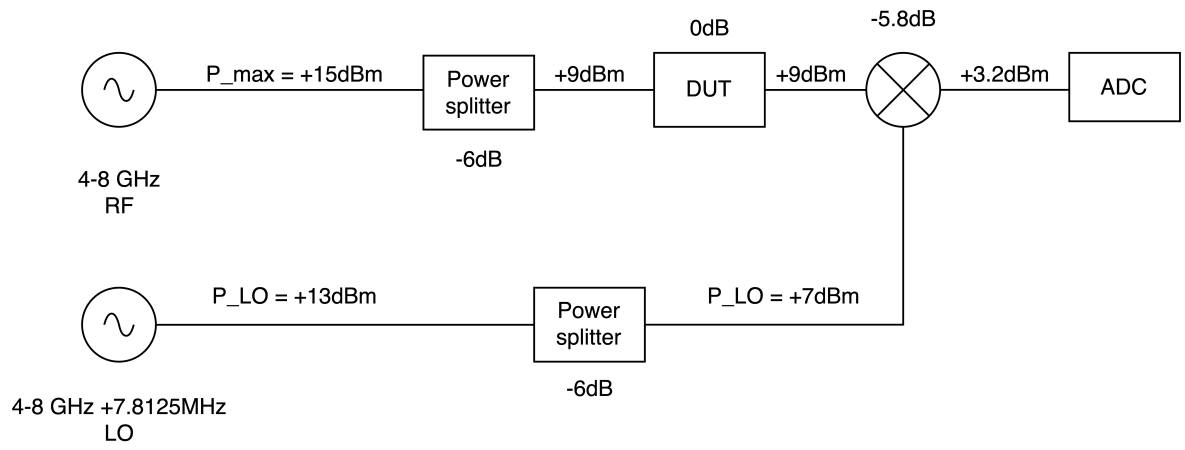

Figure 2.4: Calculation of the power levels throughout the architecture with maximum output power of the generator

Figure 2.4 illustrates the power levels throughout the architecture. It should be noted that only the DuT signal path is shown, as the power levels through both the DUT and reference paths are identical. The DuT is depicted with a gain/attenuation of 0 dB because this parameter is application-dependent.

The signal power at the input of the ADC is not equivalent to the maximum input range of the ADC ($+10$dBm). Although a gain block of $+8.8$dB could have been added, the decision was made to omit this component to reduce cost and complexity.

2.3.1. Model Limitations

It is important to emphasize that this static power implementation model is a simplified representation. Specifically, it neglects the effects of impedance mismatching and signal reflections, which can have significant impacts on the performance of RF systems. These factors are critical in actual applications and can lead to discrepancies between the modeled and actual performance of the system (this will be showed in a later chapter).

2.3.2. Component Choices

The specific components used in this architecture, including their individual losses and gains, will be discussed in subsequent chapters. These chapters will provide a detailed rationale for each component choice, ensuring that the overall system performance meets the desired specifications.

3

Generator

An RF signal generator is a fundamental component of a VNA, providing essential input to the DUT. It generates a continuous wave signal with precise frequency, amplitude and phase characteristics. Depending on the generator, certain features, such as frequency or power sweep, can be used to simulate important scenarios for the purpose of testing the DUT. This chapter presents a detailed analysis of the generator's working principle, along with a definition of the parameters that define sufficient signal quality, and a clear illustration of the measurements taken with the chosen generator.

3.1. Working principle

RF signal generators are power sources that can generate signals in the microwave range. The range used for the architecture in chapter 2 is in the C-band of the microwave spectrum [15], which is between $4-8$ GHz. In order for the generator to generate signals with high accuracy in this range, it makes use of certain features, such as phase-locked loops (PLL) and voltage controlled oscilators (VCO).

3.1.1. Phase-locked loop

The purpose of a phase-locked loop is to control the output frequency and phase of a signal until it matches the input frequency and maintains a constant phase difference, thereby locking the loop.

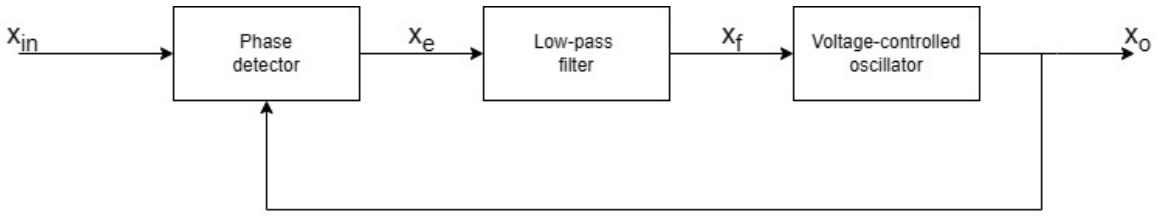

Figure 3.1: A simplified diagram of a PLL system

Figure 3.1 shows a simplified blockdiagram of a PLL. It can be seen that both the input and output are being fed into a phase detector (PD) with a feedback loop. A phase detector can also be seen as a signal multiplier. Because both the input and output are cosine waves, feeding both signals through a PD will result in two frequency components [16],

$$x_e = x_{in} \cdot x_{out} = A\cos(\omega_{in}t + \theta_{in}) \cdot B\cos(\omega_{out}t + \theta_{out}) \tag{3.1}$$

where ω is the frequency and θ is the phase. Using the trigonometric identity

$$\cos(a) \cdot \cos(b) = \frac{1}{2}[\cos(a+b) + \cos(a-b)]$$

the following expression is obtained

$$x_e = \frac{AB}{2}\cos((\omega_{in} + \omega_{out})t + \theta_{in} + \theta_{out}) + \frac{AB}{2}\cos((\omega_{in} - \omega_{out})t + \theta_{in} - \theta_{out}) \tag{3.2}$$

$$x_f = \frac{AB}{2}\cos((\omega_{in} - \omega_{out})t + \theta_{in} - \theta_{out}) \tag{3.3}$$

This expression above is also known as the error of the signal x_e. After the low-pass filter the high frequency component $\omega_{in} + \omega_{out}$ will be attenuated such that only the frequency component $\omega_{in} - \omega_{out}$ is left, which can be seen in Equation 3.3. When the PLL is locked, the frequency of the output signal must be the same as the input. This can also be shown in an expression

$$x_{out} = \cos(\omega_{in} + \varphi) \tag{3.4}$$

It can be seen that the phase of the output signal x_{out} is a linear function.

$$\theta_{out} = (\omega_{in} - \omega_{out})t + \varphi \tag{3.5}$$

Finally, plugging this relation into x_f a DC signal is obtained.

$$x_f = \frac{AB}{2}\cos(\theta_{in} - \varphi) \tag{3.6}$$

Because the VCO, as the name implies, is voltage controlled, feeding a DC signal in that is varying between 0 (when $\theta_{in} - \varphi = 90°$) and $\frac{AB}{2}$ (when $\theta_{in} = \varphi$) will control the error via the feedback loop until the PLL is locked.

Together with frequency synthesizers (which include frequency dividers and multipliers), filters, and variable amplifiers, a frequency- and power-controlled generator can be obtained. These components work together to ensure precise control and stability of the generated signal.

3.2. Defining generator signal quality

The quality of the generated signal is of utmost importance for the RF circuit. Because the generated signal will be used to perform the ratiometric measurements, it is necessary to get a clear wave for both the reference signal and the signal passing through the DUT. In order to obtain a clear waveform, it's essential to understand how the quality of an RF signal is defined. This quality can be outlined by a few essential parameters. These parameters include harmonics, spurs, signal-to-noise ratio (SNR), phase noise, and adjacent channel interference (ACI). Each parameter is briefly explained below.

- **Harmonics** are frequencies that are integer multiples of a fundamental frequency in a signal. They are often caused by nonlinearities in the system. With a fundamental frequency f_{in} the harmonics looks like:

  $$f_{out} = f_{in} + \sum_{n=2} n \cdot f_{in} \tag{3.7}$$

  The upper boundary of the summation is defined by the system itself. The quality of the harmonics is defined by subtracting the highest harmonic power from the carrier power in dB scale.

- **SNR** is a parameter that measures the ratio between the power of the fundamental signal and the power of background noise. The SNR can be defined with the following formula.

  $$SNR = P_c - P_n, \tag{3.8}$$

  where P_c is the power of the carrier and P_n is power of the noise.

- **Spurs** are unwanted frequencies generated by an RF system that are not harmonically related to the fundamental signal. The quality of the system concerning the spurs can be defined with the same formula as the SNR, but instead of the P_n, this variable will be P_s (power of the highest spur). This is also know as Spurious free dynamic range (SFDR).

- **Adjacent channel interference** can occur when a signal generator has at least two channels. Because almost all signal generators with two or more channels exist on one interconnected PCB, leakage between channels can occur. Two types of ACI exist [17]. The first occurs when the signal from channel A leaks within the bandwidth of channel B, and the second occurs when it is outside the bandwidth of channel B.
- **Phase noise** refers to the short-term, random fluctuations in the phase of a signal. In the frequency domain, it appears as sidebands (or 'skirts') around the carrier frequency, indicating deviations from the ideal carrier [18]. Phase noise is measured with different offsets from the carrier to illustrate the severity of the sidebands around the carrier.

In short, to ensure top-notch RF signal quality for ratiometric measurements, it's crucial to focus on key factors like harmonics, SNR, spurs, adjacent channel interference, and phase noise. Tackling these aspects carefully guarantees clear and accurate signals for precise analysis such that it increases the reliability of the RF circuit's performance.

3.3. Windfreaktech generator

The first generator considered was the *WindFreakTech SynthHD (v2)*. It is a dual-channel microwave generator capable of generating signals ranging between 10 MHz and 15 GHz and powers between -30dB to 20dB [19]

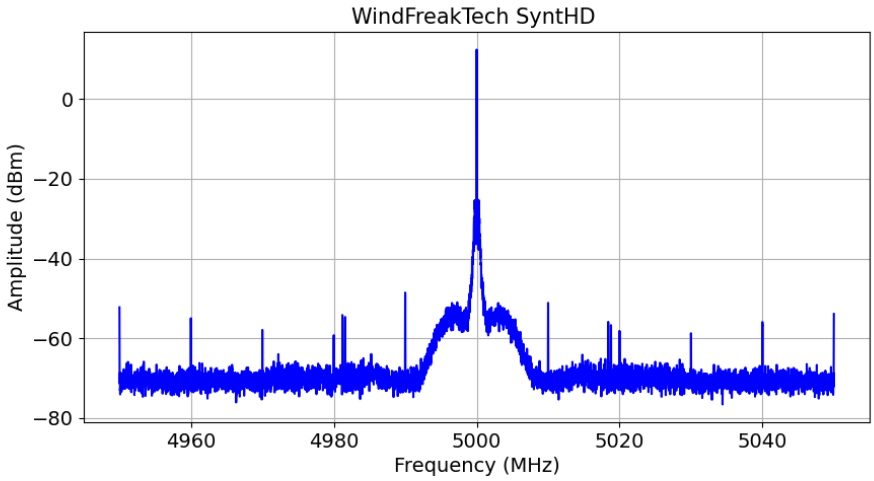

Figure 3.2: Windfreaktech SynthHD RF generator captured by SignalHound signal analyser, locked with signal analyser 10MHz reference with output power of 12dBm.

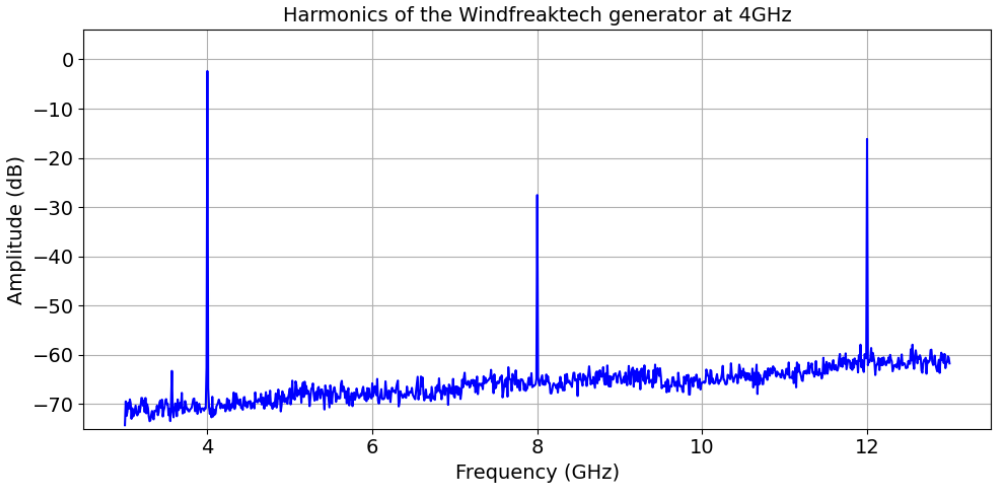

Figure 3.3: Windfreaktech SynthHD harmonics at 4GHz fundamental frequency with input power of 0dBm, captured with the Fieldfox signal analyser

Figure 3.2 shows the measurement of the output signal of the Windfreaktech generator. The spikes at 10MHz intervals around the carrier frequency of 5GHz are the spurious response of the generator. It could be caused by the reference clock leakage, or it might also be artifacts of the RF signal generation. However, the spurs are sufficiently low in relation to the carrier (below -40dBC) that it will not pose a problem for the application. Furthermore the harmonics of the WindFreakTech can be seen in Figure 3.3. Here the highest harmonic has a power of -14.15dBm while the carrier has a power of -0.36dBm. The SFDR for the WindFreakTech at 4GHz is thus 13.79dBC and does not meet requirement 5. Although the spurs do not pose a threat to the signal quality, the harmonics definitely will. Figure 3.2 also shows the skirt around the carrier. The skirt has an amplitude of -51.75dBm or 68.8dBc and is well within the accepted range. As explained before, the phase noise can be measured with different offsets. But because the highest power within the skirt is well within the accepted range, it is not necessary to show it at different offsets from the carrier.

3.4. Hittite HMC-T2100

Another generator suggested for this project is the Hittite HMC-T2100 capable of generating frequencies between 10MHz to 20GHz an power levels ranging from -36dBm to 27dBm [20].

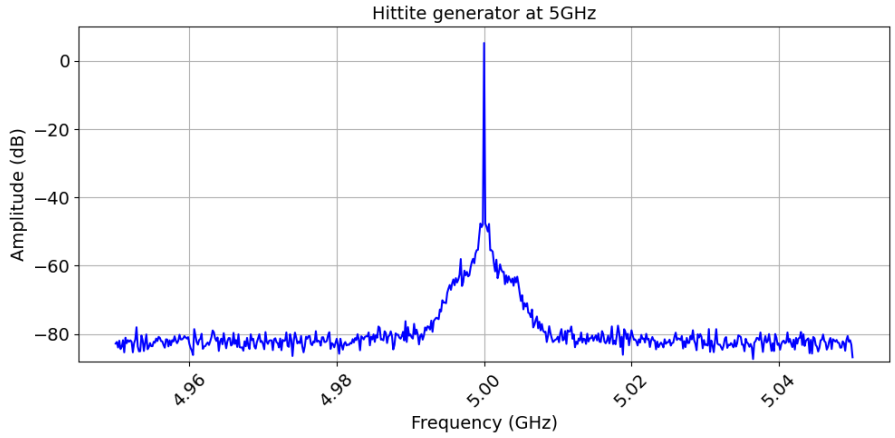

Figure 3.4: Hittite HMC-T2100 RF generator captured by Fieldfox signal analyzer. Generator is reference locked to the external 10MHz clock of the Fieldfox.

In figure 3.4 the spectrum of the Hittite is shown. The generator was set to output 5GHz at 6dBm.

The plot shows that the output power of the generator is around the input value but the actual value is 5.21dBm. This is as expected due to cable loss, connector mismatch and other related effects. At this generator the phase noise is also visible. But the same with the Windfreaktech generator, because of the low amplitude of the phase noise, it is not important to show the amplitude of the phase noise at different offsets. Another thing that can be observed from the plots is the absence of significant spurious responses. In the frequency analysis of the Windfreaktech generator significant frequency peaks could be seen around the carrier. The absence of these spurs indicate that the generated signal is of high quality and suitable for the application. Lastly, this generator only has one harmonic, which indicates also that it is of good quality.

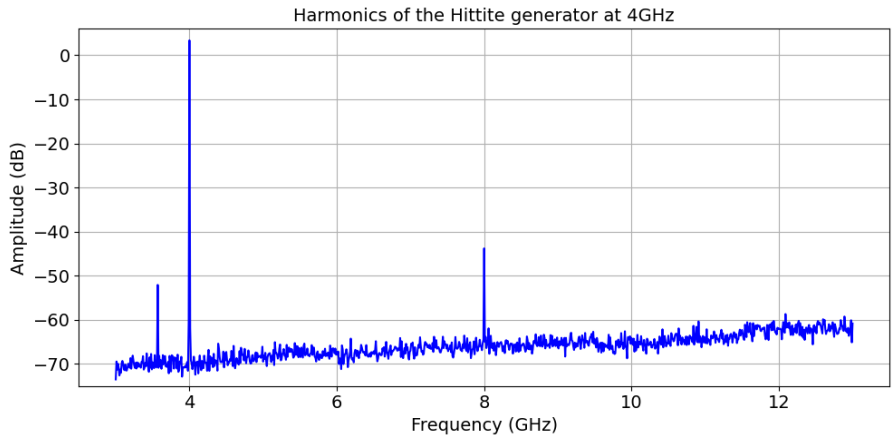

Figure 3.5: Harmonics of the Hittite generator with 4GHz as fundamental frequency ad 6dBm power, captured with the Fieldfox signal analyser

3.5. Anapico APUASYN20

The Anapico APUASYN20 RF generator is capable of generating frequencies ranging between 8kHz to 20GHz and power level variable between −10dBm to 23dBm [21].

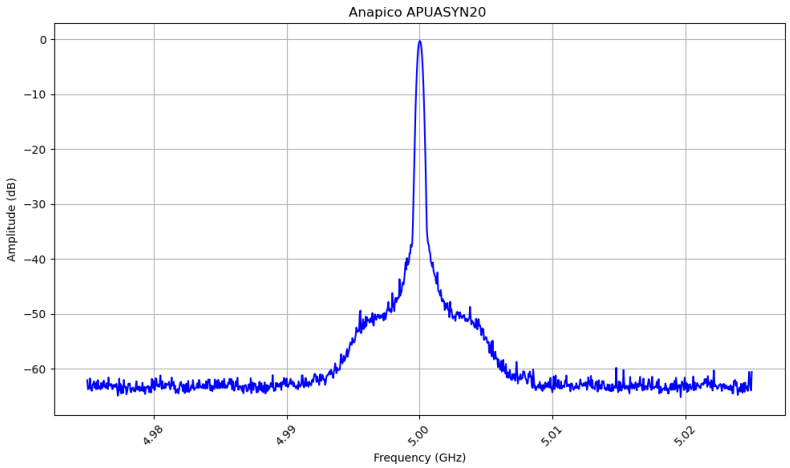

Figure 3.6: Anapico APUASYN20 RF generator captured by Fieldfox signal analyzer. Generator is reference locked to the external 10MHz clock of the Fieldfox.

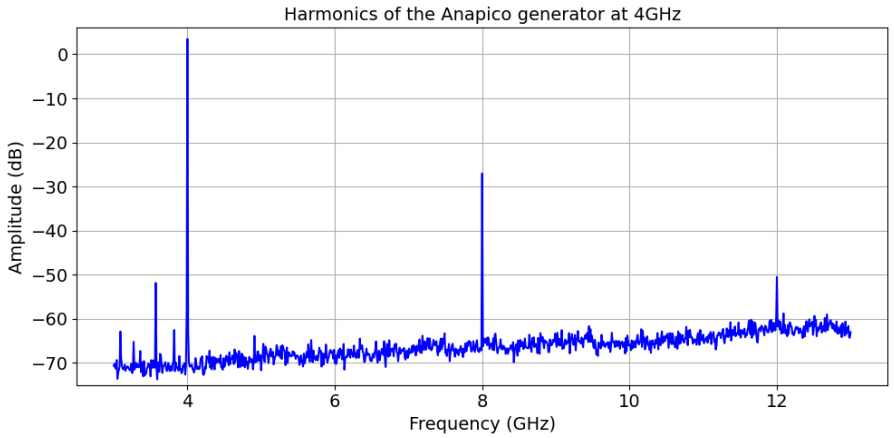

Figure 3.7: Harmonics of the Anapico generator with 4GHz as fundamental frequency ad 6dBm power, captured with the Fieldfox signal analyser

The same analysis as in section 3.4 holds for the Anapico, the signal looks almost identical to that generated by the hittite and is therefore also very well suited for VNA application. The power of the highest harmonic for the Anapico at 4GHz is -25.03dB while the carrier has a power of 5.49dB. Consequently, the power relative to the carrier is 30.50dBc and meets requirement 5.

3.6. Importance of clock locking

The importance of locking devices together can be seen in Figure 3.8. The graph on the left shows a slightly shifted carrier, an offset of 116.6kHz to be precise. This is a result of not locking the clocks together. Because crystal oscillators inside the devices always comes with a typical but rather small offset, the difference in clocks between the devices will gradually shift over time. The offset for the not clock-locked signal is smaller for the Anapico (Figure 3.9), 26.6kHz to be precise, but it is still available.

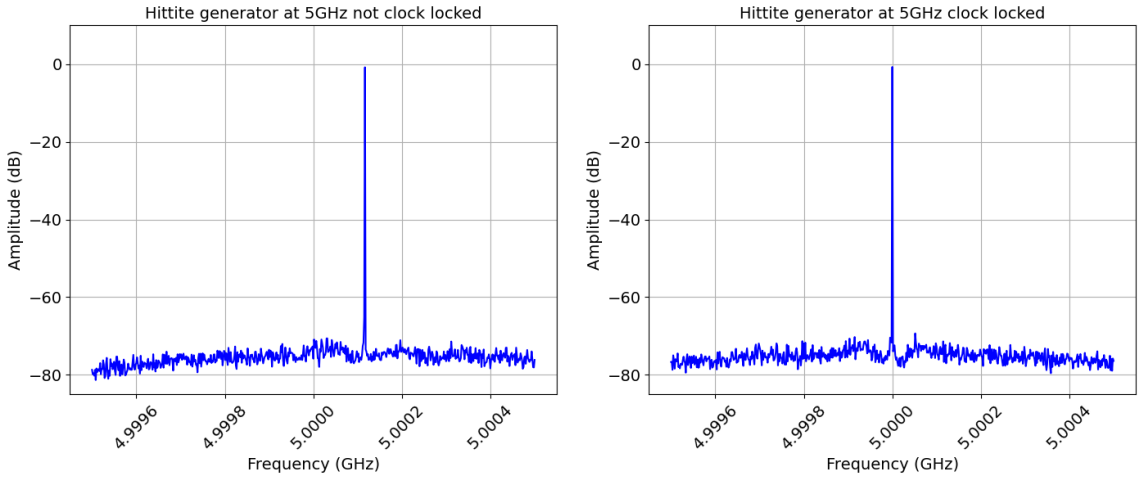

Figure 3.8: Hittite generator outputting 5GHz at 4dBm captured with the Fieldfox signal analyser. Graph on the left is not clock-locked and graph on the right is clock-locked

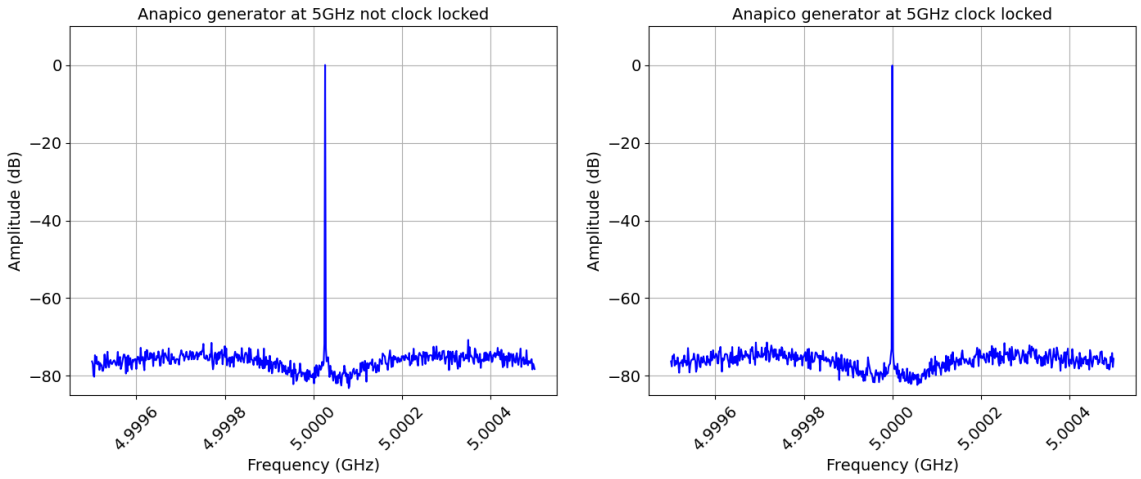

Figure 3.9: Anapico generator outputting 5GHz at 0dBm captured with the Fieldfox signal analyser. Graph on the left is not clock-locked and graph on the right is clock-locked

3.7. Design choice

Based on the measurements of the generators and the functional requirements of the system a decision was made to choose the Anapico and the Hittite for the prototype. Both generators are of sufficient quality that they meet the requirements of the system (namely requirement 2 and 4). A benefit of using the Anapico and Hittite is that the modularity and interchangeability of the system can be shown. Both generators can function as both the local oscillator and the RF generator.

4

RF Mixers

The working principle and theory behind mixers are briefly explained in section 2.1. This chapter will elaborate further on how the mixer technology used for this project works and the design choices made regarding the mixer.

4.1. Working principle of diode mixers

There are many mixer technologies available. A few of them are single/double/triple balanced diode mixers, resistive mixers, IQ mixers and transistor mixers. The most popular mixers are the passive mixers [22] and namely diode mixers. Below a circuit diagram is shown of a double balanced ring diode mixer.

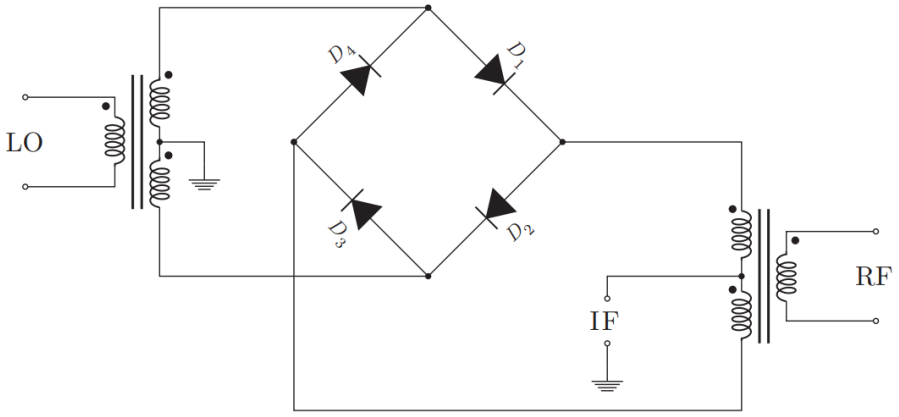

Figure 4.1: A circuit diagram of a double balanced ring diode mixer [23]

The fact that it is double balanced can be seen from the two transformers connected to the LO and RF ports. If the LO and RF port have the same signal as input, the IF output will have no voltage reading because of the $180°$ phase shift caused by the transformers and their orientation. But by introducing different frequencies to the LO and RF port, there will be a nonzero voltage across the diagonal diodes (D1-D3 and D2-D4) by only conducting during specific parts of the signal cycle and consequently the LO and RF signals are mixed and outputted at the IF port [24].

4.2. Defining mixer quality

Before making the decision to choose a mixer, it is important to first specify how mixer quality is defined. Below a few important parameters are explained.

- **P1dB** is the point at which the behaviour of the mixer deviates from being linear to being non-linear [23]. This power refers to the RF power.
- **LO power level** is the specified and required LO power in the datasheet to ensure good mixing behaviour.
- **Port-to-port isolation** defines how well a port is protected from leakage from another port.
- **Conversion loss** defines the power efficiency of the mixer with respect to the RF and IF.

4.3. Mini-circuits mixers

The function requirements specified that off-the-shelf RF components should be used. RF mixer circuits fabricated by Mini-Circuits were the most accessible. Below a table is given with the parameters mentioned in section 4.2 of the two mixers.

Mixer	RF-LO range [GHz]	IF range [GHz]	P1dB [dB]	LO power level [dB]	LO-RF isolation [dB]	LO-IF isolation [dB]	Conversion loss [dB]
ZMX-8GH	3.7 - 8	DC - 2	14	17	40	18	5.8
ZMX-10G+	3.7 - 10	DC - 2	1	7	30	17	5

Table 4.1: The datasheet parameters of the Mini-Circuits ZMX-8GH and ZMX-10G+ frequency mixers.

Both mixers operate within the required frequency range, except for the last step of the LO frequency when it is 8GHz $+ IF$. This frequency is outside the range of the ZMX-8GH mixer. Both mixers satisfy the IF frequency requirement of 7.8125MHz. However, the ZMX-8GH has an LO power that is 10dB higher compared to the ZMX-10G+. This higher LO power causes a problem at the pre-splitting stage of the architecture, as shown in Figure 2.4. To supply 17dB of power to the mixer, accounting for the loss of the power splitter (6dB), a power output of $17 + 6 = 23$dBm is needed. This power demand eliminates the Windfreaktech and Anapico generators because the required power lies outside their power level range. Additionally, this would endanger the modularity of the system and thus requirement 5 of the complete system, as not all generators can output this level of power. Moreover, the LO-RF and LO-IF isolation of both mixer are good enough to satisfy requirement 5 of the subsystem. Lastly, the conversion loss of 5dB and 5.8dB is typical [22] for passive mixers.

4.4. Downconverted IF measurements

After defining the mixer quality parameters and indicating limitations of both mixers, results of the IF are given in Figure 4.2 for ZXM-8GH and in Figure 4.3 for ZXM-10G+. Because of the stability of the system, the spectrum of the IF for RF at 4GHz and at 8GHz for both mixers are almost identical. A slight decrease in the second harmonic of mixer ZXM-8GH for RF at 8GHz can be seen and thus the minimum SFDR can be traced from the plot of RF at 4GHz for the ZXM-8GH and at 8GHz for the ZXM-10G+. The minimum SFDR of the ZXM-8GH is 21.55dBc and for the ZXM-10G+ it is 30.77dBc. For requirement 5 regarding the highest harmonic being less then 30dBc is only met with the ZXM-10G+ mixer.

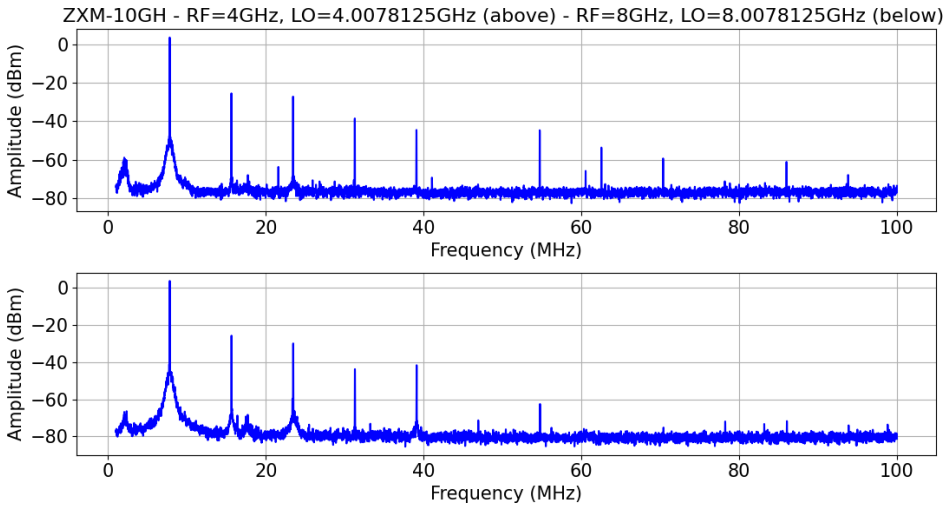

Figure 4.3: Downconverted IF signal for upper and lower RF and LO frequencies with ZMX-10G+ mixer. Anapico generator is used as the LO and the Hittite is used as RF generator.

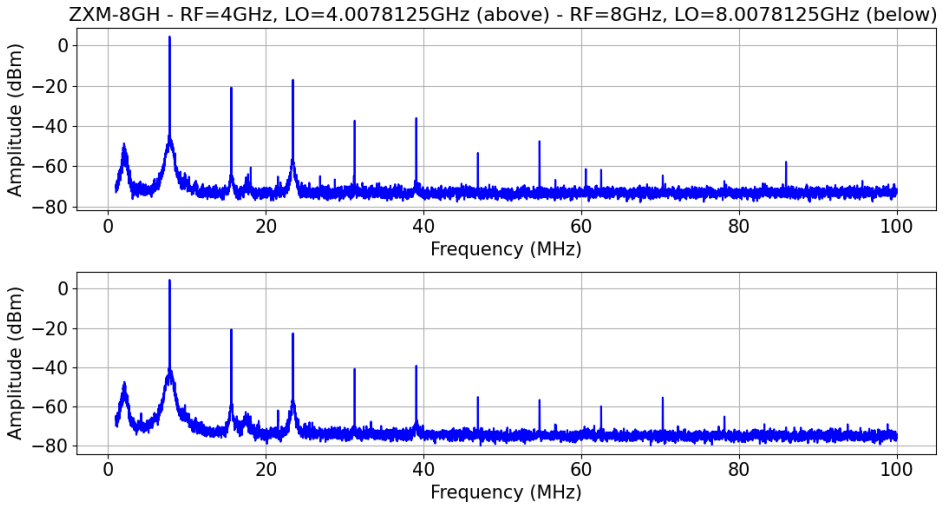

Figure 4.2: Downconverted IF signal for upper and lower RF and LO frequencies with ZMX-8GH mixer. Anapico generator is used as the LO and the Hittite is used as RF generator.

As for the phase noise of the signal, measurements were made at 4GHz, 6GHz and 8GHz for both mixers. The skirt of ZXM-8GH in figure 4.4 is wider compared to the ZXM-10G+. The highest phase noise power compared to the carrier is 51.97dBC for ZXM-8GH and 52.89dBc for ZXM-10G+. Although the phase noise difference is small between the two mixers, the ZXM-10G+ performs better.

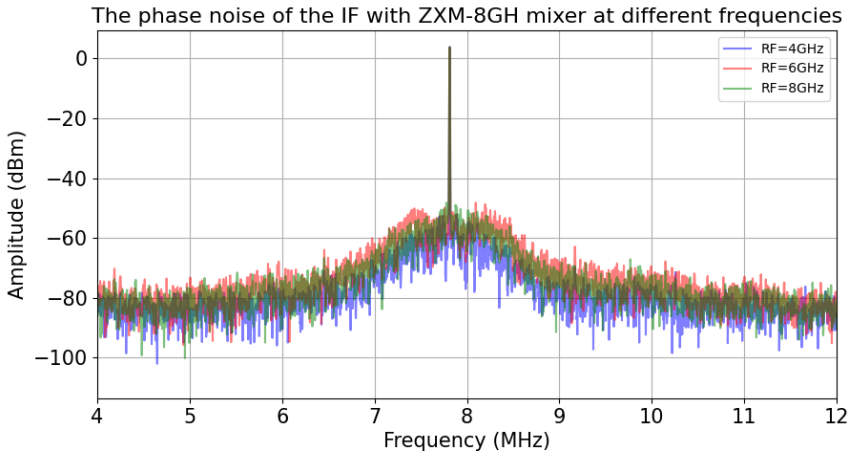

Figure 4.4: Phase noise of the IF signal at different frequencies with ZXM-8GH mixer

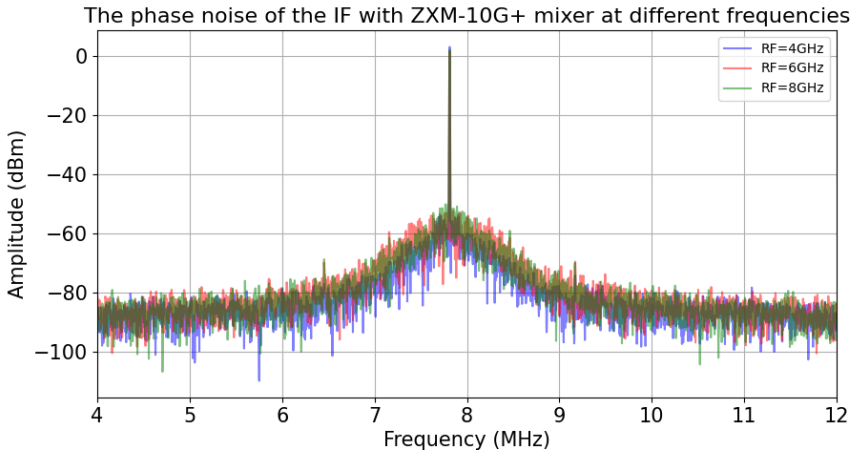

Figure 4.5: Phase noise of the IF signal at different frequencies with ZXM-10G+ mixer

4.5. Mixer design choice

A detailed comparison was made between the two mixers. For the parameters of RF-LO frequency range, LO power level, harmonics, and phase noise, the ZXM-10G+ performed far better than the ZXM-8GH. Although both mixers could be used, aiming for the best SNR is of utmost importance, and the ZXM-10G+ meets this requirement.

5

Cable connection and transmission lines

Working at high frequencies can introduce various unwanted behaviours, which can significantly impact the performance and reliability of RF systems. One of the primary concerns at high frequencies is the occurrence of delay and reflections, which can distort the signal and lead to inaccuracies. Understanding and managing these inaccuracies are essential to ensure optimal performance in RF systems. This chapter will explain the effects of such delays and how to prevent these phenomena from causing inaccuracies in the system.

5.1. Theory

As explained in the introduction, electrical systems at high frequencies carry additional problems. Before showing any measurements, it is important to introduce and explain the terms that can cause inaccuracies in the system.

- **Propagation delay** describes the time it takes the signal to go from one point to another. It can vary depending on the frequency and can cause phase errors.
- **Phase delay** refers to the time shift (or shift in phase) between the input and output of the cable.
- **Attenuation** weakens the signal and depends on factors such as material, frequency, temperature
- **Reflections** happens when a signal undergoes an impedance mismatch or change in medium, causing a portion of the signal to bounce back in the opposite direction.

5.1.1. Propagation delay

The propagation delay is expressed as:

$$t_d = \frac{d}{u_p}\ [s], \tag{5.1}$$

where d is the length of the cable in m and u_p the phase velocity of the signal in $\frac{m}{s}$. The velocity of the signal in a certain medium is given with the following formula [25]:

$$v_p = \frac{1}{\sqrt{\mu_0 \mu_r \cdot \epsilon_0 \epsilon_r}}\ [m/s] \tag{5.2}$$

The dielectric constant ϵ_r varies depending on the material, while the relative permeability $\mu_r \approx 1$ [25] for diamagnetic (weakly repelled by magnetic field) and paramagnetic substances (weakly attracted by magnetic field).

5.1.2. Phase delay calculation

Phase delay is the concept that describes the time it takes for a specific phase point to propagate through a medium or system. It can be expressed with the formula [26]

$$t_p = -\frac{\theta(\omega)}{\omega}\ [s], \tag{5.3}$$

where t_p is the phase delay in seconds, ω the angular frequency in radians and $\theta(\omega)$ the phase shift in terms of angular frequency.

Another inaccuracy that can occur due to the behaviour of coaxial cables are phase shifts.

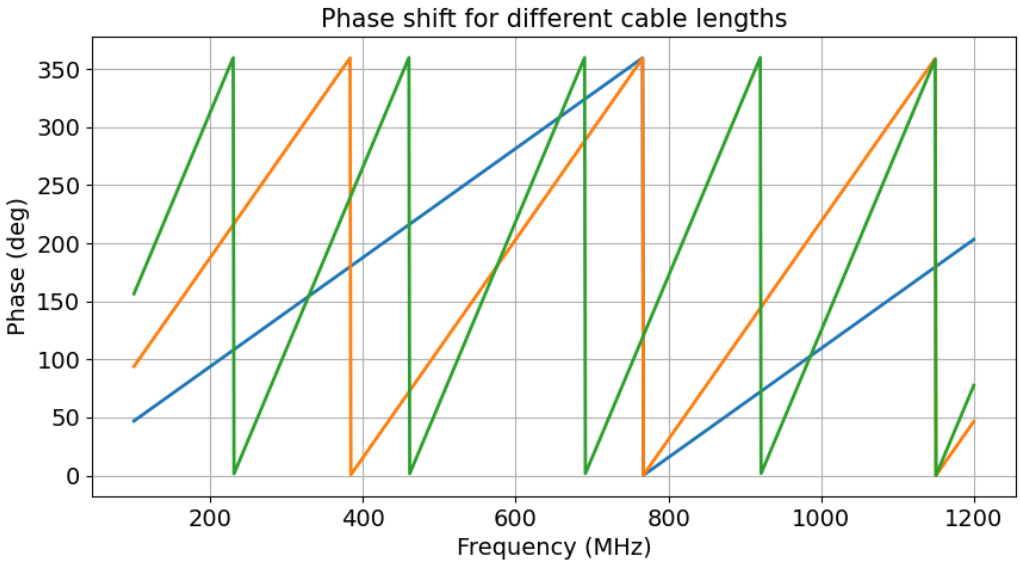

Figure 5.1: Simulation of phase offset as a function of frequency, ϵ_r was taken to be 1.7 which is typical for a coaxial cable with low loss PTFE conductor [27]

Figure 5.1 shows a theoretical plot of how the phase plots should look like. By finding the slope of the phase plots, $\theta(\omega)$ can be found and thus the phase delay.

5.1.3. Attenuation

Each signal experiences attenuation if it propagates through a passive system. Attenuation refers to the reduction of signal strength due to factors such as resistive losses, dielectric losses and radiation losses. In datasheets, attenuation is often displayed in dB as a unit of power. The loss of a incident signal can be calculated as follows:

$$P_{out} = P_{in} - P_{loss}\ [dBm], \tag{5.4}$$

where P_{out} and P_{in} are in dBm.

5.1.4. Reflection and return loss

Reflection is the phenomenon that describes the effect of a signal bouncing back to the medium it came from and can be expressed with this simple formula

$$\Gamma = \frac{V_{reflected}}{V_{incident}}, \tag{5.5}$$

where Γ is the voltage reflection coefficient [25]. Another way to express reflection is return loss (RL). Unlike equation 5.5, return loss expresses the ratio between incident wave and reflected wave in decibel

scale. A return loss of for example 30dB means that the reflected wave is 30dB less than the wave that passes through the medium. This relation is described with the formula below.

$$RL = -20\log_{10}(|\Gamma|) \tag{5.6}$$

5.2. Inaccuracies of the coaxial cables

For the RF architecture three different cables were used. The cables used are given below.

- Mini-Circuits FL141-12SM+ [28]
- Mini-Circuits FL141-24SM+ [29]
- Mini-Circuits FLC-1M-SMSM+ [30]

All the cables have a low-loss dielectric PTFE layer.

5.2.1. Phase delay measurement

In order to measure the phase delay of the signal through the cables, three measurements were made. Figure 5.2 shows the plot of three graphs. It was made by the Hittite generator generating signals with frequencies ranging from 100-1200 MHz that is fed through a two way power splitter [31]. The reason for this frequency range is due to the limitations of the oscilloscope (Rohde&Schwarz RTO 1014). One output of the splitter is used as a reference that is directly connected to the input of the oscilloscope while the other output had different cable lengths (30cm, 60cm and 100cm). With this setup, the phase shift (relative to the signal which is directly connected to the oscilloscope) due to longer cable connection can be measured.

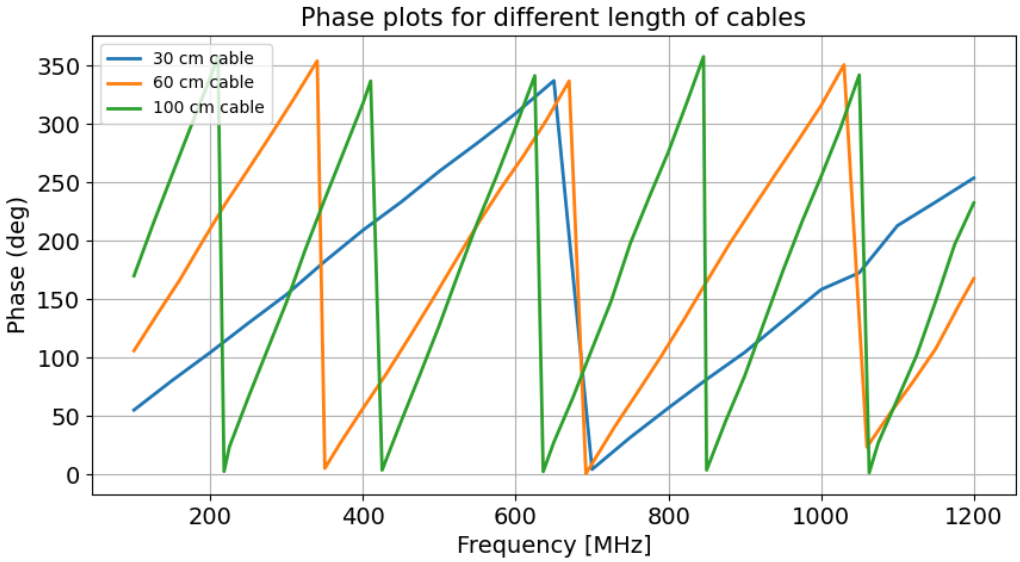

Figure 5.2: Phase plots through the SMA cable with different lengths

The phase shift shown in 5.2 is plotted modulo 360 degrees. Comparing the measurement to 5.1 it can be seen that the simulations line up quite accurately with the data. Calculating the slope, $\theta(\omega)$ can be found.

	Phase slope [Deg / MHz]	**Phase slope [Deg / Rad/s]**
θ_{30}	0.5081	8.086e-8
θ_{60}	1.0343	16.461e-8
θ_{100}	1.6818	26.766e-8

Table 5.1: The phase slopes of each cable length

The phase equation is a linear equation. By formulating a linear function with the angular frequency ($\theta(\omega)$ in equation 5.3) and dividing this by the variable ω, the phase delay is equal to the slope of the phase plot. So consequently the phase delays for each cable are shown in the table below.

Cable length	t_p [ns]
30cm	0.08086
60cm	0.16461
100cm	0.26038

Table 5.2: The phase delays of different cable lengths

Note that if the relative phase shift is $360°$, it will show as no phase delay in the measurements. So the phase delays in table 5.2 is the phase difference between the reference and different cables.

5.2.2. Propagation delay

The cables of Mini-circuits containt low-loss PTFE as dielectric. The dielectric constant for this type of material is 1.7 [27]. Using equation 5.1 and with the ϵ_r and μ_r known, the propagation delay can be found. With

$$v_p = \frac{1}{\sqrt{1.7 \cdot \epsilon_0}} = 257,751.48[m/s] \tag{5.7}$$

the propagation delay for the different cable lengths are shown below.

Cable	t_d $[\mu s]$
30cm	1.164
60cm	2.328
100cm	3.880

Table 5.3: The propagation delays of different cable lengths

5.2.3. Insertion losses

The insertion losses are detailed in the datasheets of the cables. These losses are specified over a given frequency range. The insertion losses for the frequency range of interest are presented below.

- The 30cm cable has an insertion loss of 0.25dB at 4GHz and 0.42dB at 8GHz
- The 60cm cable has an insertion loss of 0.49dB at 4GHz and 0.77dB at 8GHz
- The 100cm cable has an insertion loss of 0.91dB at 4GHz and 1.28dB at 8GHz

5.2.4. Reflection

The return losses are also provided in the datasheets of the cables. These losses are specified within a particular frequency range. The return losses for the frequency range of interest are presented below.

- The 30cm cable has an return loss of 31dB at 4GHz and 28dB at 8GHz.
- The 60cm cable has an return loss of 34dB at 4GHz and 30dB at 8GHz.
- The return loss of the 100cm cable is not defined in the datasheet.

5.3. Design choices

This chapter talked about the different effects the cable can have on the signal by taking very significant parameter into account. The effect of some parameters weigh more then others. Because the architecture has a symmetrical layout, meaning the RF side and LO side has the same components, except for the path through the DuT, making the cable lengths on both side the same the effects of phase and propagation delay can be prevented. In terms of insertion loss, the 30cm cable has the lowest loss in the frequency range of the RF. And finally the reflection can be prevented by placing a 2dB attenuator before inputs of components with high reflection (or low return loss). This way the reflection going back

to the source is attenuated one time and the reflection going from the source back into the system is attenuated twice. Overall, sticking with the shortest cable would result the best outcome in terms of signal to noise ratio.

6 Results

6.1. Cavity resonator single frequency measurements

6.1.1. Method

The first result of the full system was a test with a single frequency. The objective was to see if the basic principle of measuring the S_{21} parameter is possible with current design. In figure 6.1 the experimental setup is described. The power output of the Windfreaktech is +15dBm and the output power of the Hittite is +13dBm.

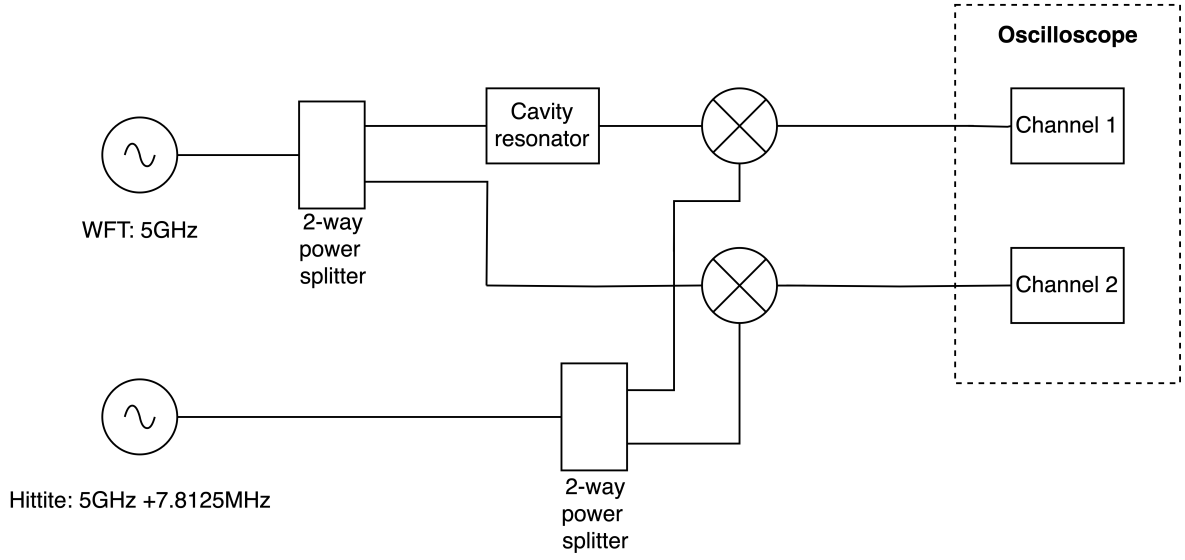

Figure 6.1: Caption

6.1.2. Data analysis

In Figure 6.2, the result of the experiment is shown. When the cavity is tuned to RF, a significant decrease in amplitude can be observed. Unfortunately, this experiment is not suitable for phase difference measurements. In Figure 6.3, a general phase and magnitude response of a cavity resonator is depicted. When the resonator is tuned exactly to RF, the expected phase offset is 0 radians. Similarly, when the cavity is tuned far away from RF, we also expect to see a 0 radians phase difference. This is precisely what is evident from the plots; only the magnitude is affected.

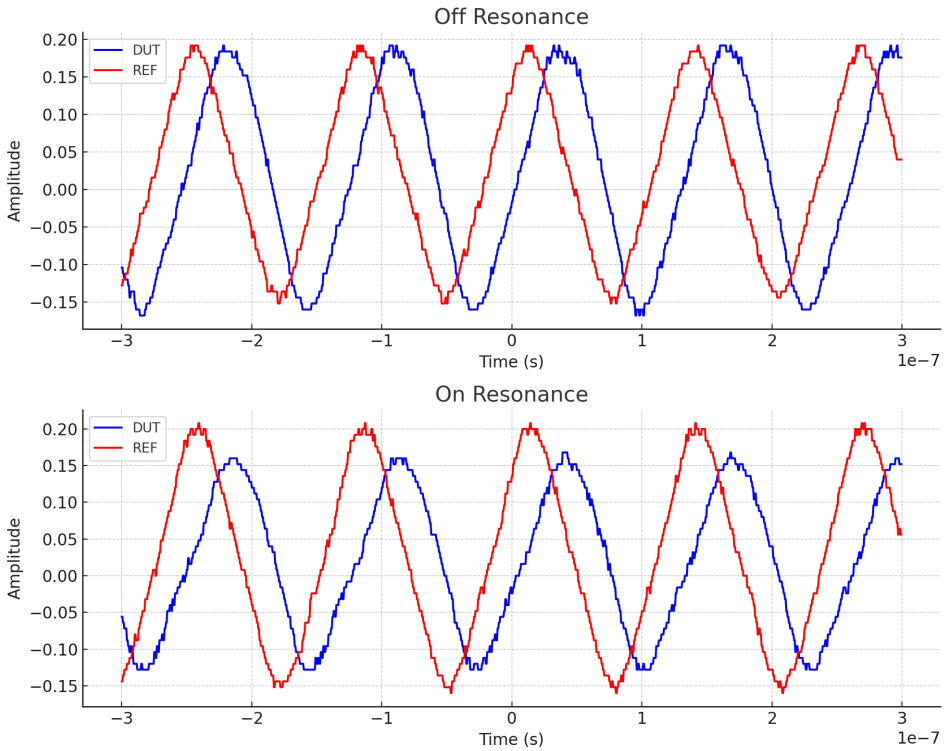

Figure 6.2: Caption

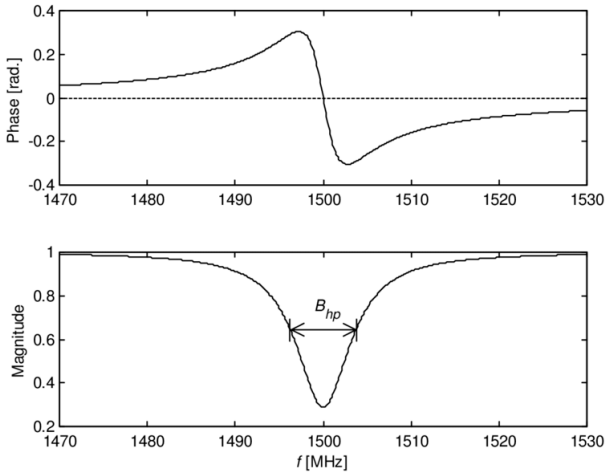

Figure 6.3: [32] Magnitude phase plot showing the response of a cavity resonator like the one used in the test experiment

From the data it is also important to know how accurate the power budget calculation has been. The REF signal in figure 6.2 is analysed. The maximum amplitude is 0.2V. Converting this the power that had to be present at the input of the ADC gives a signal power of -4dBm. It is expected to see a signal power of +3.2dBm after the mixer. Like mentioned before, this is probably caused by mismatched impedances.

6.1.3. Interpretation

It can be concluded from this first experiment that the setup is capable of sensing the magnitude change caused by the cavity resontor. The power budget is also verified and have shown that component mismatch (and related effects) cause a loss of about 7dB.

6.2. Cavity resonator swept measurement

The second measurment which verifies the working of the RF section is very similar to the previous measurement. The setup is identical only here instead of having the generators output a single frequency, the generators sweep from 4-8GHz (with a total sweep time of 20 seconds). The result from the downconversion is a constant IF (relative magnitude and phase change depending on the DUT response). The cavity resonator was tuned at approximately 6.68GHz.

A practical limitation of this experiment has been that the internal memory of the oscilloscope is too small to store all datapoints of the 20 sec trace. The data presented here works with data downsampled to 50Hz.

The settings of the Generators/sweep are as follows:

- Anapico
  - power 13dBm
  - start frequency: 4GHz
  - stop frequency: 8GHz
  - stepsize: 10 mHz
  - step time: 50 ms
- Hittite
  - power: 7dBm
  - start frequency: 4.001 GHz
  - stop frequency: 8.001 GHz
  - stepsize: 10 MHz
  - step time: 50 ms

In figure 6.5 the resulting envelope of the IF signals can be seen. At the 6.68GHz a dip is visible and this dip corresponds with the response of the cavity resonator. From the figure it can be noted why it is important to have a reference channel which uses the same power splitters, cables and mixer. Both the reference and DuT channel show the same general frequency response, if the DuT envelope is divided by the REF signal, the common behaviour is omitted (this is caused by imperfections in the RF components).

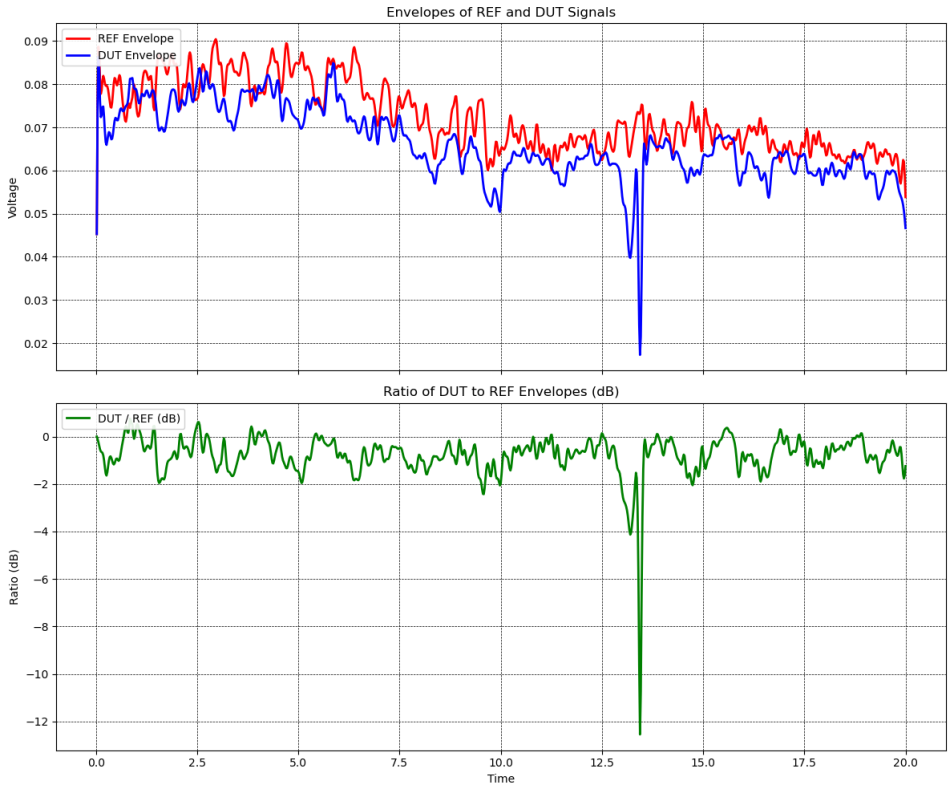

Figure 6.4: Envelope of the downconverted signals from a sweep. a) shows the two signals presented at the input of the oscilloscope (or at the ADC of the integrated system).b) shows the ratio of DUT to REF.

To verify the result, the S_{21} parameter was measured with a commercial VNA (Fieldfox). A similar dip can be seen at 6.68GHz.

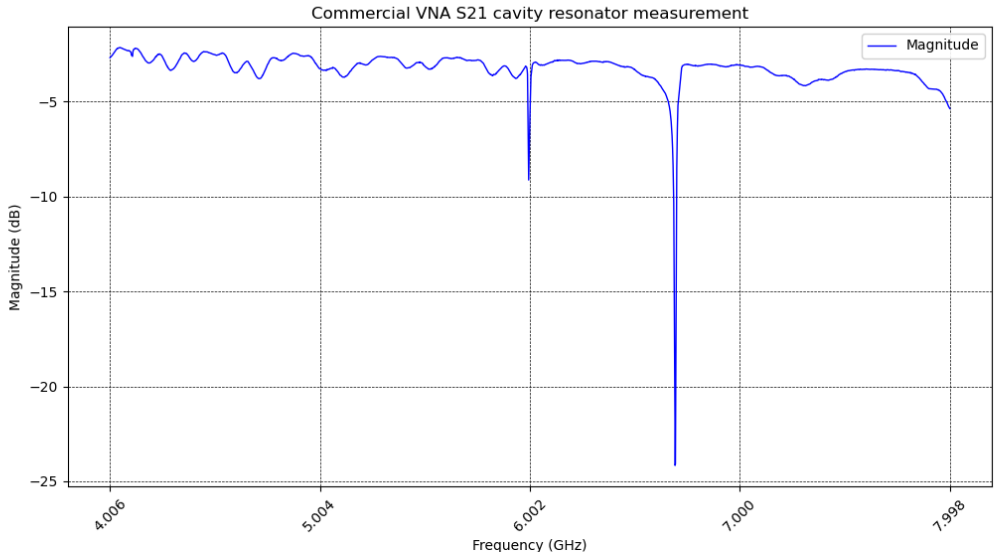

Figure 6.5: Measurement with a commercial VNA (Field Fox).

6.2.1. Narrow frequency spectrum

To better asses the functionality another measurement was done with different sweep settings, it was important to see the result for a smaller frequency sweep and to compare this to a commercial VNA. The measurement below has been made with the following generator/sweep settings:

- Anapico
  - power 13dBm
  - start frequency: 6.6GHz
  - stop frequency: 6.8GHz
  - stepsize: 1 mHz
  - step time: 100 ms
- Hittite
  - power: 7dBm
  - start frequency: 6.601 GHz
  - stop frequency: 6.801 GHz
  - stepsize: 1 MHz
  - step time: 100 ms

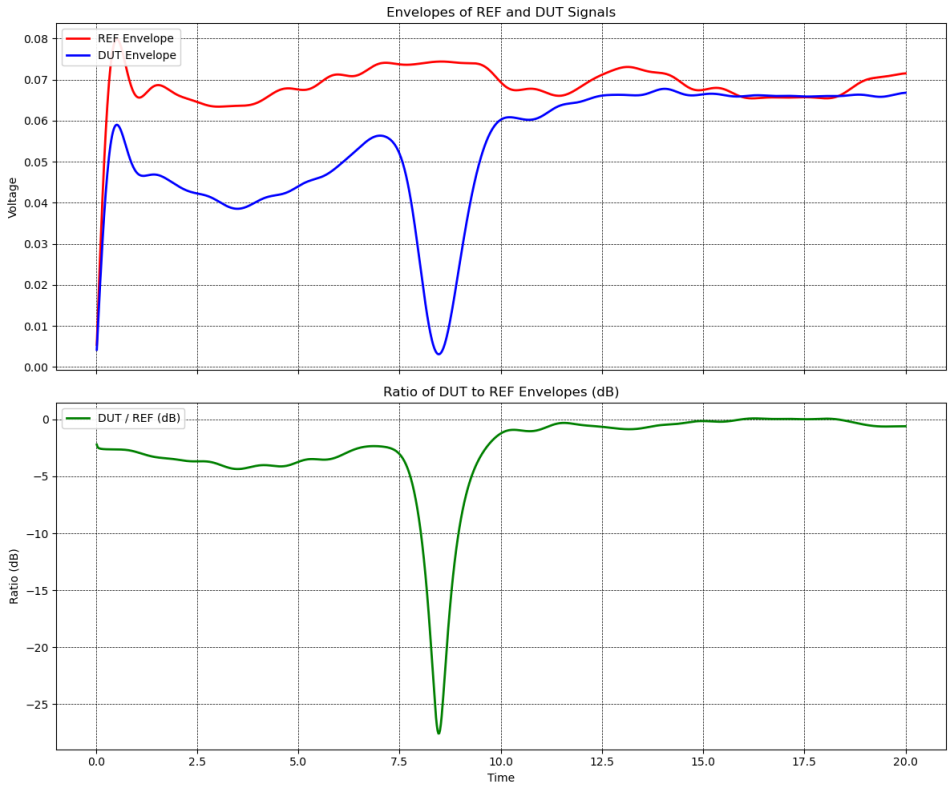

Figure 6.6: Envelope of the downconverted signals from a narrow sweep. a) shows the two signals presented at the input of the oscilloscope (or at the ADC of the integrated system).b) shows the ratio of DUT to REF.

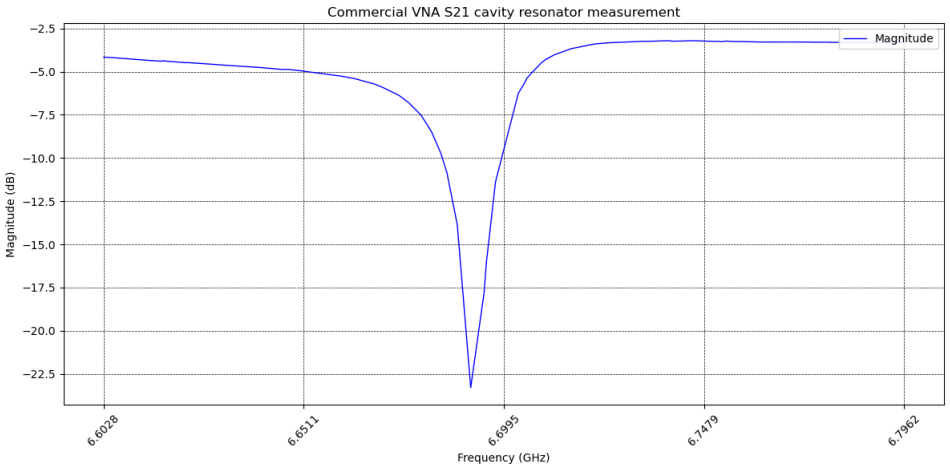

Figure 6.7: Measurement of a narrow spectrum with a commercial VNA (Field Fox).

In figure 6.6 the result of the measurement is presented. If a comparison is made between this result and the result in figure 6.7 made using the commerical VNA then it can be qualitatively concluded that the result is very similar. Thereby confirming the functioning of the RF system.

6.3. Conclusion

Looking back at the function requirements of the RF system it has been confirmed that the RF system is capable of measuring the transmission parameter S21 over a range of 4-8GHz (this is requirement 1 and 2).

7

Conclusion

In this report the design choices and measurements of the VNA RF section have been discussed. In chapter 2 the overall idea behind the architecture is presented as well as the realization of the requirement 1. By calculating the power budget throughout the system, it was discovered that the ADC input range is sufficiently high and that with maximum RF generator output (+20dBm) the ADC input would not be at its limit. In the following chapter 3 a principle of RF generations is shown and measurements of a range of generators which could be used for the application are tested and measured. All generators measured meet the signal quality requirements (spurs and harmonics). Chapter 4 followed the same structure by first explaining the principle behind RF mixers and then showing the performance measurements of the mixers. Following these performance measurement it was concluded together with the FPGA team that bandpass filtering of the IF signal is not necessary, their averaging scheme is essentially a sinc function in frequency domain with zero's at multiples of the IF frequency. The results also show that requirement 2 and 5 are met. The results section (6) demonstrates the working of the RF system. The system is able to measure the S_{21} parameter of a resonator cavity comparable to a commercial VNA. Thereby we can conclude that the RF system is fulfilling all requirements and can be used to successfully create a Vector Network Analyser.

7.1. Future work

A measurement we have not been able to do but which would be valuable is a measurement of generator frequency/phase stability over time.

Another topic that can be investigated which would add functionality to the system is the possibility of a power sweep. Our system can at the moment only sweep with a single power setting. It was mentioned that very often it is useful for quantum research to be able to sweep the power. The following engineering problems have to still be solved to make this possible

- As it is now, with maximum generator output power, the power going into (or out of the RF system) the ADC is -4dBm. With the power going to the DUT being +9dBm. Ideally when we sweep we want the voltage at the ADC to remain high (or even filled up to 1V in amplitude). A controllable variable gain amplifier could potentially be the solution.
- There are multiple locations in the signal chain where you could amplify the signal, for example, the RF signal from the DUT can be amplified, or the downconverted IF signal could be amplified. One or the other might be preferred.

References

[1] *What is a Vector Network Analyzer and How Does it Work?* [Online]. Available: https://www.tek.com/en/documents/primer/what-vector-network-analyzer-and-how-does-it-work.

[2] L. Zhong, R. Yu, and X. Hong, "Review of carbon-based electromagnetic shielding materials: film, composite, foam, textile," *Textile Research Journal*, vol. 91, p. 004 051 752 096 828, Oct. 2020. DOI: 10.1177/0040517520968282.

[3] F. Caspers, "RF engineering basic concepts: S-parameters," CERN, Tech. Rep., 2013.

[4] *What Can You Do With a VNA?* 2023. [Online]. Available: https://coppermountaintech.com/what-can-you-do-with-a-vna/.

[5] L. Dicarlo, *Introduction to circuit QED*, 2023.

[6] Keysight. "Product page: P9372A Keysight Streamline USB Vector Network Analyzer, 9 GHz." (2024), [Online]. Available: https://www.keysight.com/us/en/product/P9372A/keysight-streamline-usb-vector-network-analyzer-9-ghz.html.

[7] "About nanovna." (), [Online]. Available: https://nanovna.com.

[8] "Shfqa+ 8.5 ghz quantum analyzer." (), [Online]. Available: https://www.zhinst.com/europe/en/products/shfqa-quantum-analyzer.

[9] "Opx+: Ultra-fast quantum controller." (), [Online]. Available: https://www.quantum-machines.co/products/opx/#.

[10] A. Raza, A. Jabbar, D. A. Sehrai, H. Atiq, and R. Ramzan, "SDR Based VNA for Characterization of RF Sensors and Circuits," in *2021 1st International Conference on Microwave, Antennas & Circuits (ICMAC)*, 2021, pp. 1–4. DOI: 10.1109/ICMAC54080.2021.9678273.

[11] H. Forstén, "Improved homemade VNA," Tech. Rep., 2017. [Online]. Available: https://hforsten.com/improved-homemade-vna.html.

[12] J. Mower and Y. Kuga, "A FPGA-Based Replacement for a Network Analyzer in an Instrumentation-Based 200 GHz Radar," *High Frequency Electronics*, pp. 30–40, Sep. 2013.

[13] Y. Xu, G. Huang, N. Fruitwala, *et al.*, *QubiC 2.0: An Extensible Open-Source Qubit Control System Capable of Mid-Circuit Measurement and Feed-Forward*, 2023. arXiv: 2309.10333 [quant-ph].

[14] RS Components, *Red pitaya user manual*, 2014. [Online]. Available: https://docs.rs-online.com/84d1/0900766b8132f2ff.pdf.

[15] H. Rahman, *Fundamental Principles of Radar*. CRC Press, 2019.

[16] G.-C. Hsieh and J. Hung, "Phase-locked loop techniques. A survey," *IEEE Transactions on Industrial Electronics*, vol. 43, no. 6, pp. 609–615, 1996. DOI: 10.1109/41.544547.

[17] P. Stavroulakis, *Interference Analysis and Reduction for Wireless Systems*. Artech House, 2002, ProQuest Ebook Central. [Online]. Available: https://ebookcentral-proquest-com.tudelft.idm.oclc.org/lib/delft/detail.action?docID=227608.

[18] U. L. R. Hans L. Hartnagel Rüdiger Quay and M. Rudolph, *Fundamentals of RF and Microwave Techniques and Technologies*. Springer, 2023.

[19] *SynthHD (v2): 10MHz – 15GHz Dual Channel Microwave Generator*, SynthHD (v2), 0.1d, WindFreakTech, 2019. [Online]. Available: https://windfreaktech.com/product/microwave-signal-generator-synthhd.

[20] *HMC-T2100 SYNTHESIZED SIGNAL GENERATOR, 10 MHz to 20 GHz*, HMC-T2100, v13.1213, Analog Devices, 2013. [Online]. Available: https://www.analog.com/media/en/technical-documentation/data-sheets/hmc-t2100.pdf.

[21] *APUASYN20 Ultra-agile Frequency Synthesizer – up to 20 GHz*, APUASYN20, v1.31, Analog Devices, Nov. 2023. [Online]. Available: https://www.anapico.com/products/frequency-synthesizers/single-output-frequency-synthesizers/apuasyn20-up-to-20-ghz/.

[22] C. Nickolas, "The Basics of Mixers," *DigiKey*, 2011.

[23] C. Poole and I. Darwazeh, *Microwave active circuit analysis and design*. Academic Press, 2015.

[24] F. Electronics, *RF tutorials - Diode balanced signal mixers*, 2021. [Online]. Available: https://www.youtube.com/watch?v=iP1sqoSzn3o.

[25] U. R. F. T. Ulaby, *Fundamentals of applied electromagnetics*, 8th ed. 2022, p. 32, ISBN: 9781292436739; 1292436735.

[26] A. Ambardar, *Analog and Digital Signal Processing* (A Volume in the PWS BookWare Companion Series). PWS Pub., 1995, ISBN: 9780534940867. [Online]. Available: https://books.google.nl/books?id=JnVGAAAAYAAJ.

[27] T. S. Microwave, "HIGH PERFORMANCE MICROWAVE INTERCONNECT PRODUCTS - Dielectric options,"

[28] *Flexible Interconnect, 0.141" center diameter, 18.0 GHz*, FL141-12SM+, Rev. A, Mini-Circuits, 2018. [Online]. Available: https://www.minicircuits.com/WebStore/dashboard.html?model=FL141-12SM%2B.

[29] *Flexible Interconnect, 0.141" center diameter, 18.0 GHz*, FL141-24SM+, Rev. A, Mini-Circuits, 2018. [Online]. Available: https://www.minicircuits.com/WebStore/dashboard.html?model=FL141-24SM%2B.

[30] *Flexible Test Cable, 26.0 GHz*, FLC-1M-SMSM+, Rev. C, Mini-Circuits. [Online]. Available: https://www.minicircuits.com/WebStore/dashboard.html?model=FLC-1M-SMSM%2B.

[31] *2 Ways Resistive Power Splitter, DC - 18000 MHz, 50Ω*, ZFRSC-183-S+, Rev. D, Mini-Circuits, 2019. [Online]. Available: https://www.minicircuits.com/WebStore/dashboard.html?model=ZFRSC-183-S%2B.

[32] E. Nyfors, "Cylindrical Microwave Resonator Sensors for Measuring Materials under flow," *951-22-4983-9*,

A

List of Hardware

List of hardware used for the RF architecture and measurement purposes. (Note; not all hardware in this list is included in the proof of concept)

- Agilent Fieldfox N9916A (Vector network/Signal analyser)
- Anapico APUASYN20 (Signal generator)
- Hewlett Packard 536A (Frequency meter)
- Hewlett Packard 537A (Frequency meter)
- Hittite HMC-T2100 (Signal generator)
- Mini-Circuits FLC-1M-SMSM+ (1-meter RF cable)
- Mini-Circuits FL141-12SM+ (12-inch RF cable)
- Mini-Circuits FL141-24SM+ (24-inch RF cable)
- Mini-Circuits SLP-10.7+ (Bandpass-filter)
- Mini-Circuits ZFRSC-183-S+ (Power splitter)
- Mini-Circuits ZMX-10G+ (Frequency mixer)
- Mini-Circuits ZMX-8GH (Frequency mixer)
- Rigol DG1022 (Function generator)
- Rigol DS1064 (Oscilloscope)
- Rohde & Schwarz RTO1014 (Digital oscilloscope)
- SignalHound SA124B (Spectrum analyser)
- Windfreaktech SyntHD (v2) (Signal generator)